

**Supporting Information for
Alkynyl bridged cyclometalated Ir_2M_2 clusters: Impact of the
heterometal in the photo- and electro-luminescent properties**

Julio Fernández-Cestau,^{a,†} Nora Giménez,^a Elena Lalinde,^{a,*} Patricia Montaño,^a M. Teresa Moreno,^a Sergio Sánchez,^b Michael D. Weber,^c Rubén D. Costa ^{c,*}

^a*Departamento de Química – Centro de Investigación en Síntesis Química. Universidad de La Rioja, 26006, Logroño, Spain.*

^b*School of Chemistry, University of Manchester, Oxford Road, Manchester M13 9PL, UK*

^c*Department of Physical and Chemistry I, Excellence Cluster of Engineering of Advanced Materials (EAM), Friedrich-Alexander-Universität Erlangen-Nürnberg, Egerlandstrasse 3, 91058, Erlangen, Germany*

[†]*Present address: Wolfson Materials and Catalysis Centre, School of Chemistry, University of East Anglia, Norwich, NR4 7TJ.*

Contents:	Page
Experimental Section.....	S3
References.....	S8
Fig. S1 Selected region of the ^1H NMR in CD_3COCD_3 of $[\text{Ir}(\text{ppy})_2(\mu-\kappa C^\alpha:\eta^2-\text{C}\equiv\text{CC}_6\text{H}_4\text{OMe}-3)]_2$ (1).....	S9
Fig. S2 Selected region of the ^1H - ^1H COSY in CD_3COCD_3 of $[\text{Ir}(\text{ppy})_2(\mu-\kappa C^\alpha:\eta^2-\text{C}\equiv\text{CC}_6\text{H}_4\text{OMe}-3)]_2$ (1).....	S9
Fig. S3 Selected region of the $^{13}\text{C}\{\text{H}\}$ NMR in CD_3COCD_3 of $[\text{Ir}(\text{ppy})_2(\mu-\kappa C^\alpha:\eta^2-\text{C}\equiv\text{CC}_6\text{H}_4\text{OMe}-3)]_2$ (1).....	S10
Fig. S4. Selected region of the HSQC in in CD_3COCD_3 of $[\text{Ir}(\text{ppy})_2(\mu-\kappa C^\alpha:\eta^2-\text{C}\equiv\text{CC}_6\text{H}_4\text{OMe}-3)]_2$ (1).....	S10
Fig. S5 Selected region of the HMBC in CD_3COCD_3 of $[\text{Ir}(\text{ppy})_2(\mu-\kappa C^\alpha:\eta^2-\text{C}\equiv\text{CC}_6\text{H}_4\text{OMe}-3)]_2$ (1).....	S11
Fig. S6 Selected region of the ^1H NMR in CD_3COCD_3 of $[\text{Ir}_2\text{Ag}_2(\text{ppy})_4(\mu-\text{C}\equiv\text{CC}_6\text{H}_4\text{OMe}-3)_4]$ (2).....	S12
Fig. S7 Selected region of the ^1H - ^1H COSY in CD_3COCD_3 of $[\text{Ir}_2\text{Ag}_2(\text{ppy})_4(\mu-\text{C}\equiv\text{CC}_6\text{H}_4\text{OMe}-3)_4]$ (2).....	S12
Fig. S8 Selected region of the $^{13}\text{C}\{\text{H}\}$ NMR in CD_3COCD_3 of $[\text{Ir}_2\text{Ag}_2(\text{ppy})_4(\mu-\text{C}\equiv\text{CC}_6\text{H}_4\text{OMe}-3)_4]$ (2).....	S13
Fig. S9. Selected region of the HSQC in in CD_3COCD_3 of $[\text{Ir}_2\text{Ag}_2(\text{ppy})_4(\mu-\text{C}\equiv\text{CC}_6\text{H}_4\text{OMe}-3)_4]$ (2).....	S13
Fig. S10 Selected region of the HMBC in CD_3COCD_3 of $[\text{Ir}_2\text{Ag}_2(\text{ppy})_4(\mu-\text{C}\equiv\text{CC}_6\text{H}_4\text{OMe}-3)_4]$ (2).....	S14
Fig. S11 Selected region of the ^1H NMR in CD_3COCD_3 of $[\text{Ir}_2\text{Cu}_2(\text{ppy})_4(\mu-\text{C}\equiv\text{CC}_6\text{H}_4\text{OMe}-3)_4]$ (2).....	S15
Fig. S12 Selected region of the ^1H - ^1H COSY in CD_3COCD_3 of $[\text{Ir}_2\text{Cu}_2(\text{ppy})_4(\mu-\text{C}\equiv\text{CC}_6\text{H}_4\text{OMe}-3)_4]$ (2).....	S15

Fig. S13 Selected region of the $^{13}\text{C}\{\text{H}\}$ NMR in CD_3COCD_3 of $[\text{Ir}_2\text{Cu}_2(\text{ppy})_4(\mu-\text{C}\equiv\text{CC}_6\text{H}_4\text{OMe}-3)_4] (\mathbf{2})$	S16
Fig. S14 Selected region of the HSQC in CD_3COCD_3 of $[\text{Ir}_2\text{Cu}_2(\text{ppy})_4(\mu-\text{C}\equiv\text{CC}_6\text{H}_4\text{OMe}-3)_4] (\mathbf{2})$	S16
Fig. S15 Selected region of the HMBC in CD_3COCD_3 of $[\text{Ir}_2\text{Cu}_2(\text{ppy})_4(\mu-\text{C}\equiv\text{CC}_6\text{H}_4\text{OMe}-3)_4] (\mathbf{2})$	S17
Table S1 X-ray Crystallographic Data for 1 · $2\text{CH}_3\text{COCH}_3$, 2 · $2\text{CH}_2\text{Cl}_2$ and 3	S18
Fig. S16 Two different view of the X-ray crystal structure of 1 · $2\text{CH}_3\text{COCH}_3$	S19
Table S2 Selected Bond Lengths and Angles for 1 · $2\text{CH}_3\text{COCH}_3$	S19
Fig. S17 Two different view of the X-ray crystal structure of 2 · $2\text{CH}_2\text{Cl}_2$	S20
Fig. S18. Crystal packing of complex 2 · $2\text{CH}_2\text{Cl}_2$	S20
Table S3 Selected Bond Lengths and Angles for 2 · $2\text{CH}_2\text{Cl}_2$	S21
Fig. S19 Two different view of the X-ray crystal structure of 3	S22
Fig. S20 Crystal packing of complex 3	S22
Table S4 Selected Bond Lengths and Angles for 3	S23
Fig. S21a Cyclic voltammogram of 1 – 3 .in THF.....	S24
Fig. S21b Cyclic voltammogram of 1 in CH_2Cl_2	S24
Table S5 Absorption data (solid state and solution 10^{-4} M, 298 K) and Electrochemical Data (THF 10^{-4} M).....	S24
Fig. S22 UV-visible absorption spectra.....	S25
Table S6 Photophysical data.....	S26
Fig. S23 Normalized emission spectra in THF (10^{-4} M) at 298 and 77 K of 1	S26
Fig. S24 Normalized emission spectra of 2 a) in solid state b) in THF (10^{-4} M) at 298 K and 77 K.....	S27
Fig. S25 Normalized emission spectra of 3 a) in solid state b) in THF (10^{-4} M) at 298 K and 77 K.....	S27
Fig. S26 Emission spectra of 2 and 3 in PMMA thin films at variable concentrations (wt%) at 298K.....	S28
Table S7 DFT optimized geometries for ground state and triplet state of complex 2	S29
Table S8 DFT optimized geometries for ground state and triplet state of 3	S30
Fig. S27 Calculated absorptions bars and the low energy section of experimental UV-vis.....	S30
Table S9 Composition of Frontier Molecular Orbitals (%) in Terms of ligands and Metals in the Ground-State for 2 and 3	S31
Table S10 Selected vertical excitation energies computed by TD-DFT in CH_2Cl_2 with the orbitals involved for complexes 2 and 3	S32
Fig. S28 Frontier MOs of 2 optimized in the ground state.....	S33
Fig. S29 Frontier MOs of 3 optimized in the ground state.....	S34
Table S11 Composition of Frontier Molecular Orbitals in the Triplet state for 2 and 3 ...	S34
Fig. S30 Optimized structures (S_0 and T_1 state) in 3 .	S35

Experimental Section

General Remarks. All reactions were carried out under Ar atmosphere using Schlenk tube techniques. Solvents were obtained from a solvent purification system (M-BRAUN MB SPS-800). IR spectra were recorded on a FT-IR Nicolet Nexus spectrometer as Nujol mulls between polyethylene sheets and NMR spectra were recorded on either a Bruker Avance 400 spectrometer. Chemical shifts are reported in ppm relative to external standards (SiMe_4) and coupling constants in Hz. Elemental analyses were carried out on a Perkin-Elmer 2400 CHNS/O microanalyzer. Mass spectra were recorded on a Microflex MALDI-TOF Bruker spectrometer operating in the linear and reflector modes using dithranol as matrix. Cyclic voltammetry were carried out in 0.1 M NBu_4PF_6 solutions as supporting electrolyte, using a three-electrode configuration (Pt disk as working electrode, Pt-wire counter electrode, Ag/AgCl reference electrode) on a Voltalab PST 050. The ferrocene/ferrocenium couple served as internal reference (+0.58 V vs Ag/AgCl). The optical absorption spectra were recorded using a Hewlett-Packard 8453 (solution) spectrophotometer in the visible and near-UV range. Diffuse reflectance UV-vis (DRUV) data of pressed powder diluted with KBr were recorded on a Shimadzu (UV-3600 spectrophotometer with a Harrick Praying Mantis accessory) and recalculated following the Kubelka-Munk function. Excitation and emission spectra were obtained on a Jobin-Yvon Horiba Fluorolog 3-11 Tau-3 spectrofluorimeter. The lifetime measurements were performed in a Jobin Yvon Horiba Fluorolog operating in the phosphorimeter mode (with an F1-1029 lifetime emission PMT assembly, using a 450W Xe lamp) or with a Datastation HUB-B with a nanoLED controller and software DAS6. The nanoLEDs employed for lifetime measurements were of 390 nm with pulse lengths of 0.8–1.4 ns. The lifetime data have been fitted using the Jobin-Yvon software package. Quantum yields were measured using a F-3018 Integrating Sphere mounted on a Fluorolog 3-11 Tau-3 spectrofluorimeter. The starting materials $[\text{Ir}(\text{ppy})_2(\mu\text{-Cl})]_2$,¹ $[\text{MC}\equiv\text{CC}_6\text{H}_4\text{OMe}-3]_n$ (M= Cu, Ag)² was prepared as reported in the literature and the spectroscopic properties matched those reported. Alkynes were purchased from Aldrich.

Preparation of $[\text{Ir}(\text{ppy})_2(\mu\text{-}\kappa C^a:\eta^2\text{-C}\equiv\text{CC}_6\text{H}_4\text{OMe}-3)]_2$ (1). To a fresh (-20°C) solution of $\text{LiC}\equiv\text{CC}_6\text{H}_4\text{OMe}-3$ (1.68 mmol) in THF (20 ml), $[\text{Ir}(\text{ppy})_2(\mu\text{-Cl})]_2$ (0.300 g, 0.280 mmol) was added. The mixture was stirred at this temperature for 1 hour, and then was allowed to reach room temperature (48 h). The resulting yellow suspension was evaporated to dryness, and the final residue was treated with CH_2Cl_2 (~ 40 ml). The

orange solution was filtered under N₂ through Celite, and the filtrate was evaporated to dryness. Addition of cold EtOH (~ 5 ml) afforded as a dark yellow solid (0.216 g, 82%). Anal. Calc. for C₆₂H₄₆Ir₂N₄O₂ (1263.49): C, 58.93; H, 3.67; N, 4.43. Found: C, 59.36; H, 3.71; N, 4.36 %. IR: ν(C≡C) 1997 cm⁻¹. MALDI-TOF (+): *m/z* (%): 501 [Ir(ppy)₂]⁺ (84%), 632 [Ir(ppy)₂(C≡CC₆H₄OMe-3)]⁺ (100%), 763 [Ir(ppy)₂(C≡CC₆H₄OMe-3)₂]⁺ (57%), 977 [Ir₂(ppy)₃(C≡CC₆H₄OMe-3)]⁺ (27%), 1108 [Ir₂(ppy)₃(C≡CC₆H₄OMe-3)₂]⁺ (18%), 1148 [Ir₂(ppy)₄(C≡CC₆H₄OMe-3)(OH)]⁺ (6%). ¹H NMR (400.1 MHz, CD₃COCD₃, 298 K): δ = 9.41 (d, *J* = 5.5, 4H, H²_{ppy}), 8.00 (d, *J* = 7.3, 4H, H⁵_{ppy}), 7.83 (t, *J* = 7.3, 4H, H⁴_{ppy}), 7.50 (d, *J* = 7.3, 4H, H⁶_{ppy}), 6.93 (t, *J* = 6.5, 4H, H³_{ppy}), 6.62 (t, *J* = 6.5, 4H, H⁷_{ppy}), 6.51 (m, 6H, H⁸_{ppy}, H⁵_{C6H4}), 6.27 (dd, ³*J* = 8.1 Hz, ⁴*J* = 2.1 Hz, 2H, H⁶_{C6H4}), 5.92 (d, *J* = 7.5, 4H, H⁹_{ppy}), 5.77 (d, *J* = 7.6, 2H, H⁴_{C6H4}), 5.73 (s, 2H, H²_{C6H4}), 3.39 (s, 6H, -OMe). ¹³C{¹H} NMR (100.62 MHz, CD₃COCD₃, 298 K): δ = 169.8 (s, C¹²_{ppy}), 161.3 (s, C¹¹_{ppy}), 159.1 (s, C³_{C6H4}), 151.7 (s, C²_{ppy}), 144.6 (s, C¹⁰_{ppy}), 137.3 (s, C⁴_{ppy}), 131.0 (s, C⁹_{ppy}), 129.8 (s, C⁸_{ppy}), 128.3 (s, C⁵_{C6H4}), 124.4 (s, C⁶_{ppy}), 123.7 (s, C⁴_{C6H4}), 122.6 (s, C³_{ppy}), 121.3 (s, C⁷_{ppy}), 119.9 (s, C⁵_{ppy}), 115.6 (s, C²_{C6H4}), 112.2 (s, C⁶_{C6H4}), 103.0 (s, C_β), 80.2 (s, C_α), 55.0 (s, C_{-OMe}).

Preparation of [Ir₂Ag₂(ppy)₄(μ-C≡CC₆H₄OMe-3)₄] (2). *Method i:* To a yellow solution of [Ir(ppy)₂(C≡CC₆H₄OMe-3)]₂ (0.1 g, 0.080 mmol) in THF (60 ml) was added [AgC≡CC₆H₄OMe-3]_n (0.04 g, 0.160 mmol) at room temperature and the mixture was stirred for 24 h protected from the light. The resulting suspension was evaporated to dryness, the residue treated with CH₂Cl₂ (~40 ml) and filtered under N₂ through Celite. The solvent was eliminated from the filtrate and treated with cold n-hexane (~5 ml) to afford **2** as a yellow solid (0.130 g, 93% yield). *Method ii:* [AgC≡CC₆H₄OMe-3]_n (0.089 g, 0.373 mmol) was added to a yellow solution of [Ir(ppy)₂(μ-Cl)]₂ (0.1 g, 0.094 mmol) in THF (60 ml) and the mixture stirred for c.a. 72 h. protected from the light. The obtained AgCl was filtered off and the resulting yellow filtrate was evaporated to dryness. Addition of cold Et₂O (~5 ml) afforded **2** as a yellow solid (0.115 g, 75%).

Anal. Calc. for C₈₀H₆₀Ag₂Ir₂N₄O₄ (1741.53): C, 55.17; H, 3.47; N, 3.22 . Found: C, 54.87; H, 3.50; N, 3.57%. IR: ν(C≡C) 1990, 1964 cm⁻¹. MALDI-TOF (+): *m/z* (%): 501 [Ir(ppy)₂]⁺ (85%), 632 [Ir(ppy)₂(C≡CC₆H₄OMe-3)]⁺ (53%), 739 [IrAg(ppy)₂(C≡CC₆H₄OMe-3)]⁺, 763 [Ir(ppy)₂(C≡CC₆H₄OMe-3)₂]⁺ (100%), 979 [IrAg₂(ppy)₂(C≡CC₆H₄OMe-3)₂]⁺ (33%), 1455 [Ir₂Ag₂(ppy)₃(C≡CC₆H₄OMe-3)₃]⁺ (68%), 1480 [Ir₂Ag₂(ppy)₄(C≡CC₆H₄OMe-3)₂]⁺ (26%), 1609 [Ir₂Ag₂(ppy)₄(C≡CC₆H₄OMe-3)₃]⁺ (41%), 1742 [Ir₂Ag₂(ppy)₄(C≡CC₆H₄OMe-3)₄]⁺

(8%), 1849 $[\text{Ir}_2\text{Ag}_3(\text{ppy})_4(\text{C}\equiv\text{CC}_6\text{H}_4\text{OMe}-3)_4]^+$ (37%), 2089 $[\text{Ir}_2\text{Ag}_4(\text{ppy})_4(\text{C}\equiv\text{CC}_6\text{H}_4\text{OMe}-3)_5]^+$ (34%). ^1H NMR (400.1 MHz, CD_3COCD_3 , 298 K): δ = 9.91 (d, J = 5.7 Hz, 4H, H^2_{ppy}), 7.98 (d, J = 8.3 Hz, 4H, H^5_{ppy}), 7.67 (d, J = 8.1 Hz, 4H, H^6_{ppy}), 7.63 (t, J = 8.0 Hz, 4H, H^4_{ppy}), 7.11 (t, J = 6.8 Hz, 4H, H^3_{ppy}), 6.97 (t, J = 8.0 Hz, 4H, $\text{H}^5_{\text{C}_6\text{H}_4}$), 6.76 (m, 8H, $\text{H}^{7,8}_{\text{ppy}}$), 6.69 (dd, 3J = 8.3 Hz, 4J = 1.7 Hz, 4H, $\text{H}^6_{\text{C}_6\text{H}_4}$), 6.38 (m, 8H, H^9_{ppy} , $\text{H}^4_{\text{C}_6\text{H}_4}$), 6.33 (s, 4H, $\text{H}^2_{\text{C}_6\text{H}_4}$), 3.52 (s, 12H, -OMe). $^{13}\text{C}\{\text{H}\}$ NMR (100.62 MHz, CD_3COCD_3 , 298 K): δ = 169.0 (s, $\text{C}^{12}_{\text{ppy}}$), 159.3 (s, $\text{C}^{11}_{\text{ppy}}$, $\text{C}^3_{\text{C}_6\text{H}_4}$), 152.4 (s, C^2_{ppy}), 144.2 (s, $\text{C}^{10}_{\text{ppy}}$), 136.5 (s, C^4_{ppy}), 130.6 (s, C^9_{ppy}), 129.5, 128.9 (s, C^8_{ppy} , $\text{C}^5_{\text{C}_6\text{H}_4}$), 127.1 (s, $\text{C}^1_{\text{C}_6\text{H}_4}$), 123.8 (s, C^6_{ppy}), 123.6 (s, $\text{C}^4_{\text{C}_6\text{H}_4}$), 122.6 (s, C^3_{ppy}), 120.8 (s, C^7_{ppy}), 119.3 (s, C^5_{ppy}), 116.5 (s, $\text{C}^2_{\text{C}_6\text{H}_4}$), 112.9 (s, $\text{C}^6_{\text{C}_6\text{H}_4}$), 54.6 (s, $\text{C}_{-\text{OMe}}$).

Preparation of $[\text{Ir}_2\text{Cu}_2(\text{ppy})_4(\mu\text{-C}\equiv\text{CC}_6\text{H}_4\text{OMe}-3)_4]$ (3). To a yellow solution of $[\text{Ir}(\text{ppy})_2(\text{C}\equiv\text{CC}_6\text{H}_4\text{OMe}-3)]_2$ (0.1 g, 0.080 mmol) in THF (60 ml) was added $[\text{CuC}\equiv\text{CC}_6\text{H}_4\text{OMe}-3]_n$ (0.03 g, 0.160 mmol) at room temperature and the mixture was stirred for 72 h. The resulting suspension was evaporated to dryness, the residue treated with CH_2Cl_2 (~40 ml) and filtered under N_2 through Celite. The solvent was eliminated from the filtrate and treated with cold n-hexane (~5 ml) to afford **2** as an orange solid (0.120 g, 91% yield). Anal. Calc. for $\text{C}_{80}\text{H}_{60}\text{Cu}_2\text{Ir}_2\text{N}_4\text{O}_4$ (1652.25): C, 58.10; H, 3.66; N, 3.39. Found: C, 57.81; H, 3.75; N, 3.69%. IR: $\nu(\text{C}\equiv\text{C})$ 1952 cm^{-1} . MALDI-TOF (+): m/z (%): 501 $[\text{Ir}(\text{ppy})_2]^+$ (25%), 632 $[\text{Ir}(\text{ppy})_2(\text{C}\equiv\text{CC}_6\text{H}_4\text{OMe}-3)]^+$ (30%), 763 $[\text{Ir}(\text{ppy})_2(\text{C}\equiv\text{CC}_6\text{H}_4\text{OMe}-3)_2]^+$ (28%), 826 $[\text{IrCu}(\text{ppy})_2(\text{C}\equiv\text{CC}_6\text{H}_4\text{OMe}-3)_2]^+$ (24%), 1212 $[\text{Ir}_2\text{Cu}_2(\text{ppy})_2(\text{C}\equiv\text{CC}_6\text{H}_4\text{OMe}-3)_3]^+$ (10%), 1367 $[\text{Ir}_2\text{Cu}_2(\text{ppy})_3(\text{C}\equiv\text{CC}_6\text{H}_4\text{OMe}-3)_3]^+$ (100%), 1499 $[\text{Ir}_2\text{Cu}_2(\text{ppy})_3(\text{C}\equiv\text{CC}_6\text{H}_4\text{OMe}-3)_4]^+$ (19%), 1521 $[\text{Ir}_2\text{Cu}_2(\text{ppy})_4(\text{C}\equiv\text{CC}_6\text{H}_4\text{OMe}-3)_3]^+$ (10%), 1652 $[\text{Ir}_2\text{Cu}_2(\text{ppy})_4(\text{C}\equiv\text{CC}_6\text{H}_4\text{OMe}-3)_4]^+$ (6%), 1715 $[\text{Ir}_2\text{Cu}_3(\text{ppy})_4(\text{C}\equiv\text{CC}_6\text{H}_4\text{OMe}-3)_4]^+$ (22%). ^1H NMR (400.1 MHz, CD_3COCD_3 , 298 K): δ = 9.82 (d, J = 5.6 Hz, 4H, H^2_{ppy}), 7.81 (d, J = 7.9 Hz, 4H, H^5_{ppy}), 7.61 (m, 8H, $\text{H}^{6,4}_{\text{ppy}}$), 7.12 (t, J = 6.6 Hz, 4H, H^3_{ppy}), 6.96 (t, J = 7.7 Hz, 4H, $\text{H}^5_{\text{C}_6\text{H}_4}$), 6.77 (m, 8H, $\text{H}^{7,8}_{\text{ppy}}$), 6.69 (dd, 3J = 8.5 Hz, 4J = 1.7 Hz, 4H, $\text{H}^6_{\text{C}_6\text{H}_4}$), 6.48 (d, 3J = 7.6 Hz, 4H, $\text{H}^4_{\text{C}_6\text{H}_4}$), 6.35 (s, 4H, $\text{H}^2_{\text{C}_6\text{H}_4}$), 6.32 (d, J = 7.3 Hz, 4H, H^9_{ppy}), 3.37 (s, 12H, -OMe). $^{13}\text{C}\{\text{H}\}$ NMR (100.62 MHz, CD_3COCD_3 , 298 K): δ = 168.6 (s, $\text{C}^{12}_{\text{ppy}}$), 162.5 (s, $\text{C}^{11}_{\text{ppy}}$), 159.3 (s, $\text{C}^3_{\text{C}_6\text{H}_4}$), 152.6 (s, C^2_{ppy}), 144.1 (s, $\text{C}^{10}_{\text{ppy}}$), 136.3 (s, C^4_{ppy}), 130.4 (s, C^9_{ppy}), 128.9 (s, C^8_{ppy}), 128.8 (s, $\text{C}^5_{\text{C}_6\text{H}_4}$), 127.9 (s, $\text{C}^1_{\text{C}_6\text{H}_4}$), 123.8 (s, C^6_{ppy}), 123.3 (s, $\text{C}^4_{\text{C}_6\text{H}_4}$), 122.3 (s, C^3_{ppy}), 120.9 (s, C^7_{ppy}), 119.1 (s, C^5_{ppy}), 116.5 (s, $\text{C}_{\alpha/\beta}$), 115.7 (s, $\text{C}^2_{\text{C}_6\text{H}_4}$), 113.2 (s, $\text{C}^6_{\text{C}_6\text{H}_4}$), 107.6 (s, $\text{C}_{\alpha/\beta}$), 54.0 (s, $\text{C}_{-\text{OMe}}$).

X-Ray Crystallography. Table S1 reports details of the structural analysis for complexes **1**·2CH₃COCH₃, **2**·2CH₂Cl₂ and **3**. Yellow crystals of **1** and **2** were obtained by slow evaporation of the complexes in acetone (1·2CH₃OCH₃; room temperature) or in a 1:2 mixture of CH₂Cl₂/acetone (**2**·2CH₂Cl₂), respectively. Crystals of **3** were prepared by slow diffusion of *n*-hexane into solution of **3** in CH₂Cl₂. X-ray intensity data were collected with a NONIUS- κ CCD area-detector diffractometer, using graphite-monochromatic Mo-K α radiation, and images were processed using the DENZO and SCALEPACK suite of programs.³ The structures were solved by Direct Methods using SHELXS-97⁴ (**2**·1.5CH₂Cl₂) or Patterson and Fourier methods using DIRDIF2008⁵ (**1**·2CH₃OCH₃, **3**), and refined by full-matrix least squares on F^2 with SHELXL.⁶ The absorption corrections were performed using MULTI-SCAN⁷ (**1**·2CH₃OCH₃, **3**), or X-Abs⁸ (**2**·2CH₂Cl₂), with the WINGX program suite.⁹ For complex **2**, two crystallization CH₂Cl₂ molecules were observed. One of these molecules is model with occupancy 1. The second could not be adequately modelled and was removed from the model. Examination with PLATON¹⁰ and SQUEEZE^{10,11} revealed the presence of one void of 287 Å³ in the unit cell, containing 157 e⁻. This fits with the presence of 2 molecules of CH₂Cl₂ in the unit cell and gives rise to the stoichiometry (**2**·2CH₂Cl₂). For **3**, one methoxyphenyl ring is disordered over two positions, A and B, with group occupancies of 0.75 and 0.25, respectively. C17A, C16B, C17B, C18B and O2B atoms were introduced in the refinement isotropically. The rest of non-hydrogen atoms were assigned anisotropic displacement parameters. The hydrogen atoms were constrained to idealized geometries fixing isotropic displacement parameters of 1.2 times the U_{iso} value of their attached carbons for aromatic and methylene hydrogens and 1.5 times for the methyl groups. The structures present some residual peaks greater than 1 e Å⁻³ in the vicinity of the metal atoms, solvent molecules, and/or aromatic rings but with no chemical meaning.

Computational Details. All DFT and TD-DFT calculations were performed by the Gaussian 09 programs¹² using the range-separated and dispersion-corrected hybrid density functional wB97X-D.¹³ The basis set used for the iridium centers was the LanL2DZ effective core potential¹⁴ and 6-31G(d,p) for the ligand atoms. The ωB97X-D functional was selected for this study because it contains both long-range exchange and empirical dispersion corrections, which are important for the modeling of structures with weak interactions and localized anionic or strongly electron donating sites.¹⁵ The geometry structures were optimized in gas phase and the solvent effect of the dichloromethane in the TD-DFT calculations was taken in consideration by the

polarizable continuum model (PCM).¹⁶ The GaussSum 2.2 software¹⁷ was used to calculate group contributions to the molecular orbitals. The emission energy was calculated as the difference of the DFT-optimised T₁ geometry for both states (adiabatic electronic transition).

Device preparation and analysis. Double layer LECs were fabricated as follows.¹⁸ ITO coated glass plates were patterned by conventional photolithography (Naranjo Substrates). The substrates were cleaned by using sequential ultrasonic baths, namely in water-soap, water, ethanol, and propan-2-ol solvents. After drying, the substrates were placed in a UV–ozone cleaner (Jetlight 42-220) for 8 min. An 100 nm layer of PEDOT:PSS was doctor-bladed onto the ITO-glass substrate to increase the device preparation yield (400 µm substrate distance and a speed of 10 mm/s). The luminescent layer was prepared by depositing a mixture of CBP and the emitter in a mass ratio 80:20 in THF (20 mg/mL). The active layer was deposited by means of spin-coating (700 rpm for 1 min) reaching a thickness of 90-100 nm. These conditions resulted in homogenous thin films with a roughness less than 5 %, having no apparent optical defects. The latter was determined using the profilometer DektakxT from Bruker. Once the active layer was deposited, the samples were transferred into an inert atmosphere glovebox (<0.1 ppm O₂ and H₂O, Innovative Technology). Aluminum cathode electrode (75 nm) was thermally evaporated using a shadow mask under high vacuum (<1·10–6 mbar) using an Angstrom Covap evaporator integrated into the inert atmosphere glovebox. Time dependence of luminance, voltage, and current was measured by applying constant and/or pulsed voltage and current by monitoring the desired parameters simultaneously by using Avantes spectrophotometer (Avaspec-ULS2048L-USB2) in conjunction with a calibrated integrated sphere Avasphere 30-Irrad and Botest OLT OLED Lifetime-Test System. Electroluminescence spectra were recorded using the above mentioned spectrophotometer.

References

- 1 M. Mauro, G. De Paoli, M. Otter, D. Donghi, G. D'Alfonso and L. De Cola, *Dalton Trans.* 2011, **40**, 12106.
- 2 G. van Koten and J. G. Noltes, In *Comprehensive Organometallic Chemistry*, Vol. 2. (Eds.: Wilkinson, F. G. A. Stone, E. Lebel), Pergamon Press, Oxford: 1982, p 721.
- 3 Z. Otwinowski and W. Minor, In *Methods in Enzymology*, C. V. Carter Jr., R. M. Sweet, Eds. Academic Press: New York, 1997; Vol. 276A, pp 307.

- 4 G. M. Sheldrick, *SHELX-97, a Program for the Refinement of Crystal Structures*. University of Göttingen: Germany, 1997.
- 5 P. T. Beursken, G. Beursken, R. de Gelder, J. M. M. Smits, S. García-Granda and R. O. Gould, *DIRDIF2008.*, Crystallography Laboratory, Radboud University Nijmegen, Toernooiveld 1, 65525 ED Nijmegen, The Netherlands, 2008
- 6 G. M. Sheldrick, *Acta Crystallogr., Sect. C* 2015, **71**, 3.
- 7 R. H. Blessing, *Acta Crystallogr.* 1995, **A51**, 33.
- 8 S. Parkin, B. Moezzi and H. Hope, *J. Appl. Cryst.*, 1995, **28**, 53.
- 9 L. J. Farrugia, *J. Appl. Crystallogr.* 1999, **32**, 837.
- 10 A. L. Speck, *J. Appl. Cryst.*, 2003, **36**, 7.
- 11 (a) A. L. Speck, *Acta Crystallogr., Sect C*, 2015, **71**, 9. (b) A. L. Speck, *Acta Crystallogr.*, 1990, **A46**, C.
- 12 Gaussian 09, Revision B.01, M. J. Frisch, G. W. Trucks, H. B. Schlegel, G. E. Scuseria, M. A. Robb, J. R. Cheeseman, G. Scalmani, V. Barone, B. Mennucci, G. A. Petersson, H. Nakatsuji, M. Caricato, X. Li, H. P. Hratchian, A. F. Izmaylov, J. Bloino, G. Zheng, J. L. Sonnenberg, M. Hada, M. Ehara, K. Toyota, R. Fukuda, J. Hasegawa, M. Ishida, T. Nakajima, Y. Honda, O. Kitao, H. Nakai, T. Vreven, J. A. Montgomery, Jr., J. E. Peralta, F. Ogliaro, M. Bearpark, J. J. Heyd, E. Brothers, K. N. Kudin, V. N. Staroverov, T. Keith, R. Kobayashi, J. Normand, K. Raghavachari, A. Rendell, J. C. Burant, S. S. Iyengar, J. Tomasi, M. Cossi, N. Rega, J. M. Millam, M. Klene, J. E. Knox, J. B. Cross, V. Bakken, C. Adamo, J. Jaramillo, R. Gomperts, R. E. Stratmann, O. Yazyev, A. J. Austin, R. Cammi, C. Pomelli, J. W. Ochterski, R. L. Martin, K. Morokuma, V. G. Zakrzewski, G. A. Voth, P. Salvador, J. J. Dannenberg, S. Dapprich, A. D. Daniels, O. Farkas, J. B. Foresman, J. V. Ortiz, J. Cioslowski, and D. J. Fox, Gaussian, Inc., Wallingford CT, 2010.
- 13 J. D. Chai and M. Head-Gordon, *Phys. Chem. Chem. Phys.* 2008, **10**, 6615.
- 14 W. R. Wadt and P. J. Hay, *J. Chem. Phys.* 1985, **82**, 284.
- 15 (a) F. Jensen, *J. Chem. Theory Comput.* 2010, **6**, 2726; (b) K. S. Thanthiriwatte, E. G. Hohenstein, L. A. Burns and C. D. Sherrill, *J. Chem. Theory Comput.* 2011, **7**, 88.
- 16 V. Barone and M. Cossi, *J. Phys. Chem. A* 1998, **102**, 1995.
- 17 N. M. O'Boyle, A. L. Tenderholt and K. M. Langner, *J. Comp. Chem.* 2008, **29**, 839.
- 18 (a) A. J. Norell Bader, A. A. Ilkevich, I. V. Kosilkin and J. M. Leger, *Nano Lett.*, 2011, **11**, 461; (b) A. Pertegas, N. M. Shavaleev, D. Tordera, E. Orti, M. K. Nazeeruddin and H. J. Bolink, *J. Mat. Chem. C*, 2014, **2**, 1605; (c) G. Qian, Y. Lin, G. Wantz, A. R. Davis, K. R. Carter and J. J. Watkins, *Adv. Funct. Mat.*, 2014, **24**, 4484; (d) S. Tang, H. A. Buchholz and L. Edman, *J. Mat. Chem. C*, 2015, **3**, 8114.

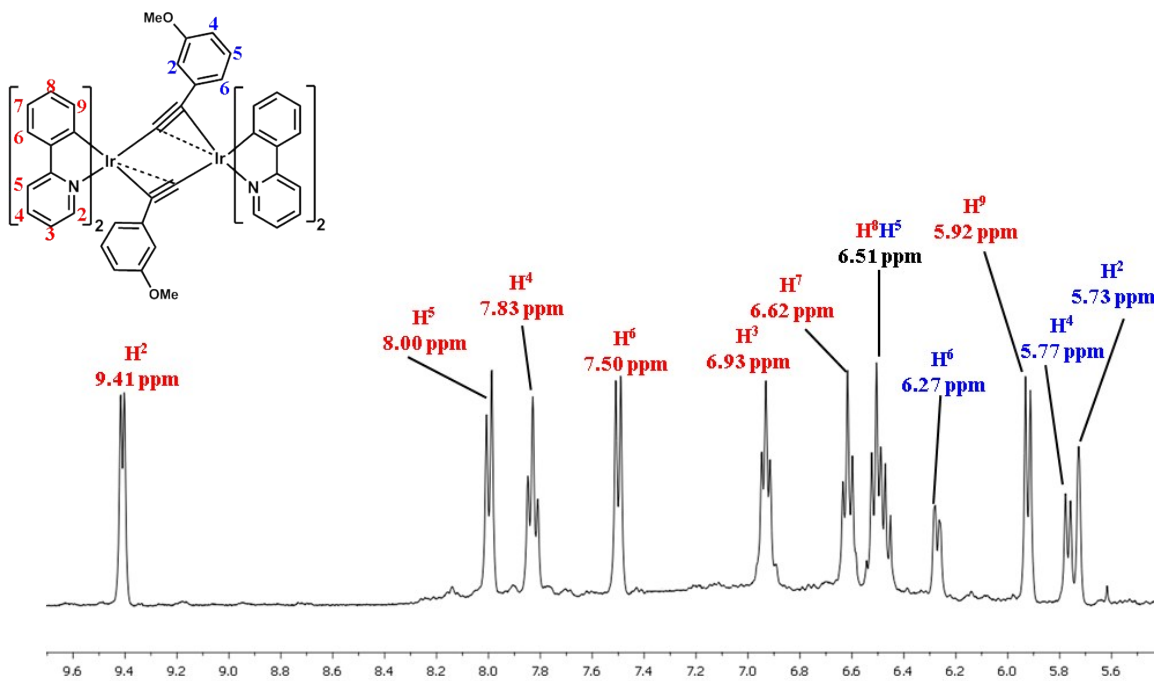


Fig. S1 Selected region of the ¹H NMR in CD₃COCD₃ of complex [Ir(ppy)₂(μ-κC^a:η²-C≡CC₆H₄OMe-3)]₂ (**1**)

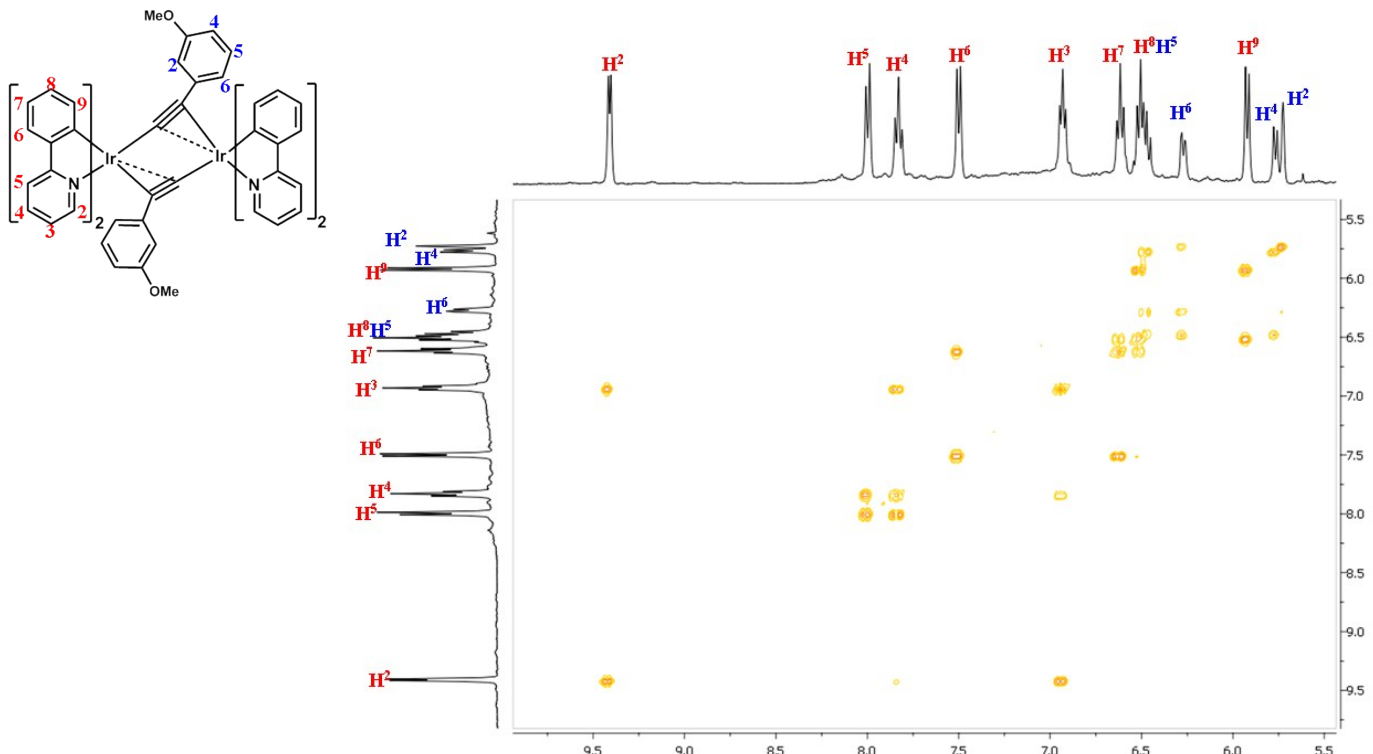


Fig. S2 Selected region of the ¹H-¹H COSY in CD₃COCD₃ of complex [Ir(ppy)₂(μ-κC^a:η²-C≡CC₆H₄OMe-3)]₂ (**1**)

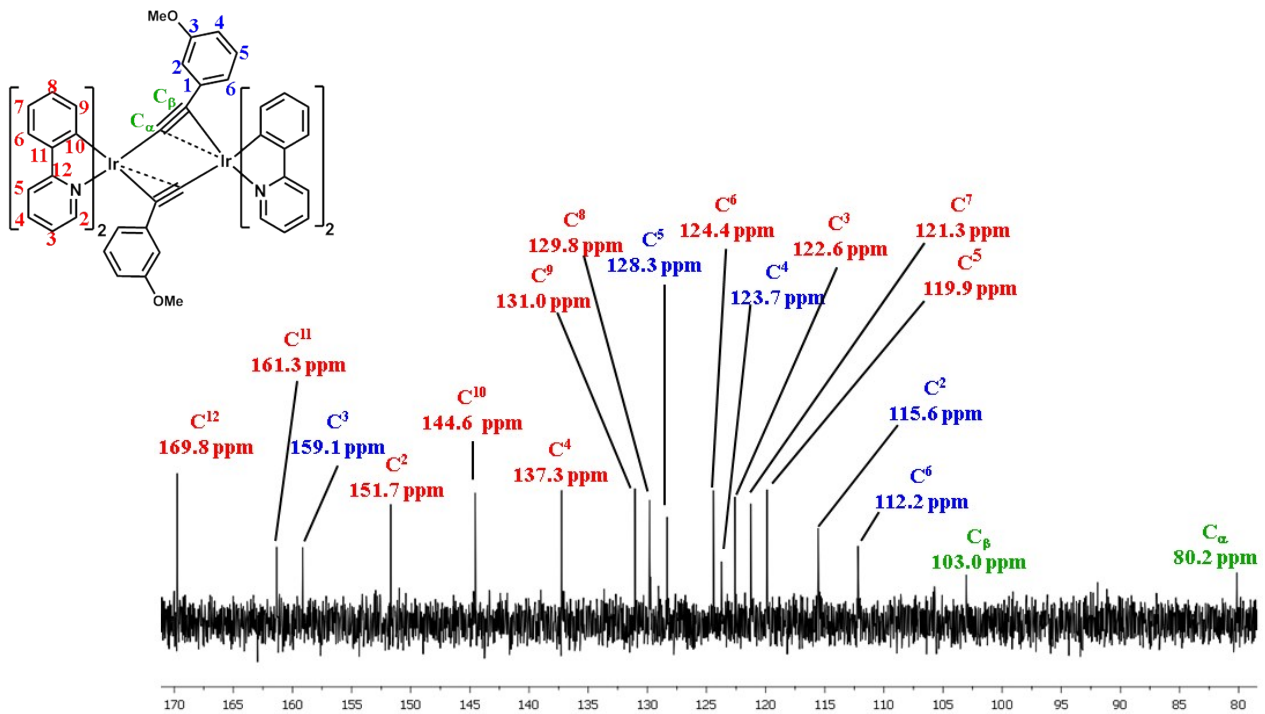


Fig. S3 Selected region of the $^{13}\text{C}\{\text{H}\}$ NMR in CD_3COCD_3 of complex $[\text{Ir}(\text{ppy})_2(\mu-\kappa\text{C}^\alpha:\eta^2-\text{C}\equiv\text{CC}_6\text{H}_4\text{OMe}-3)]_2$ (1)

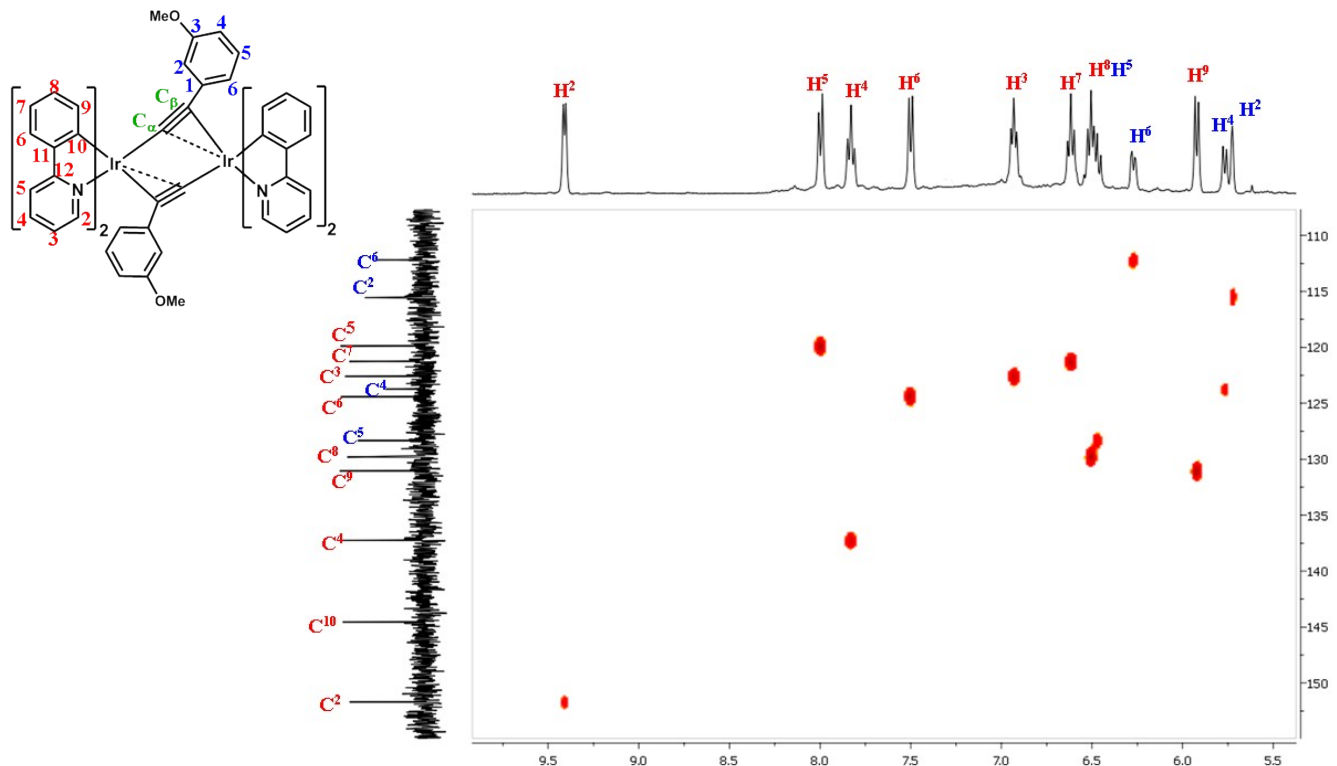


Fig. S4 Selected region of the HSQC in CD_3COCD_3 of complex $[\text{Ir}(\text{ppy})_2(\mu-\kappa\text{C}^\alpha:\eta^2-\text{C}\equiv\text{CC}_6\text{H}_4\text{OMe}-3)]_2$ (1)

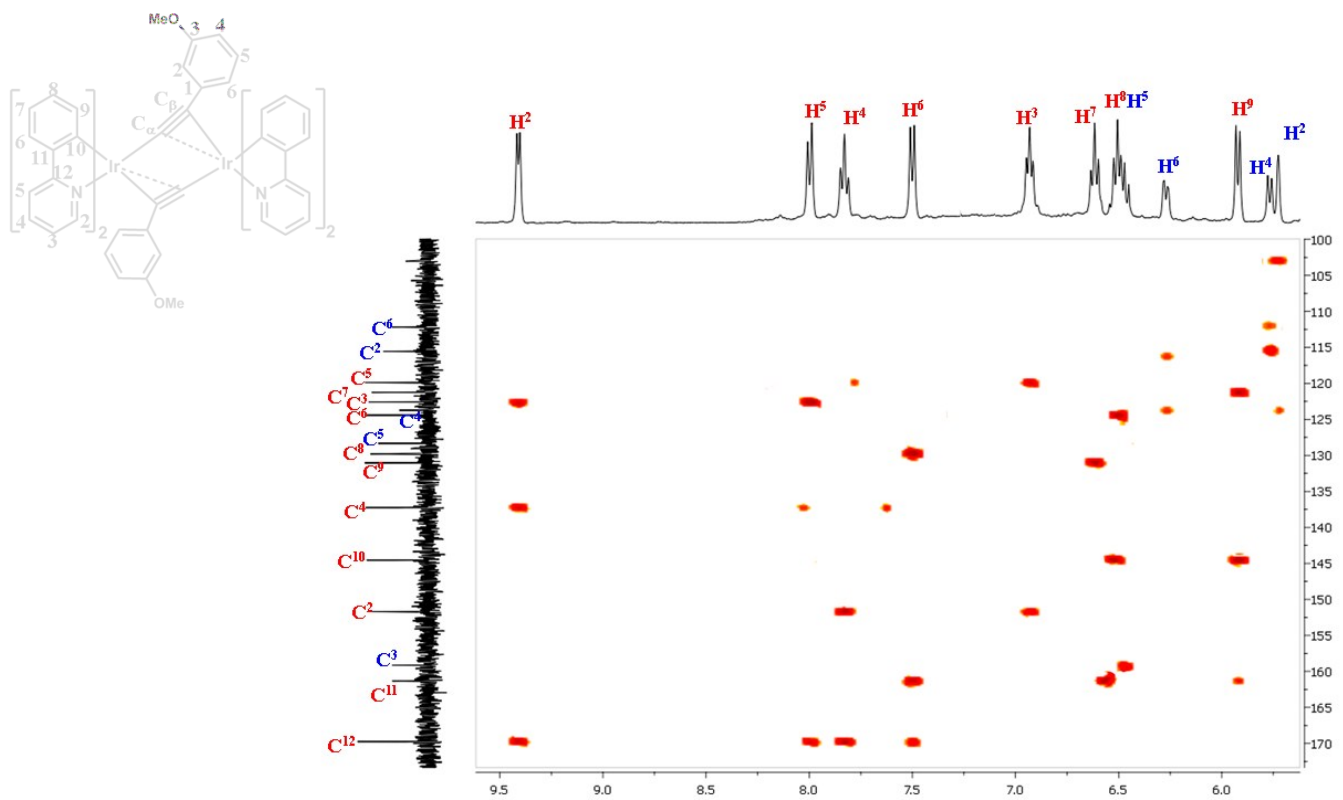


Fig. S5 Selected region of HMBC the in CD_3COCD_3 of complex $[\text{Ir}(\text{ppy})_2(\mu\text{-}\kappa C^{\alpha}:\eta^2\text{-}C\equiv\text{CC}_6\text{H}_4\text{OMe-3})]_2$ (**1**)

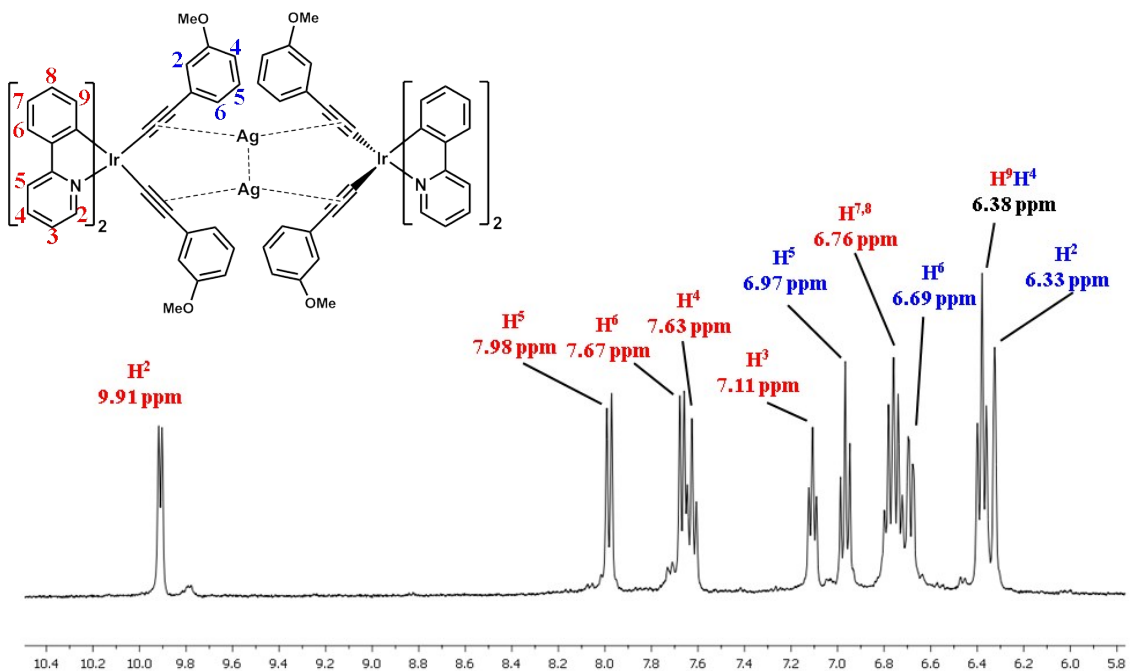


Fig. S6 Selected region of the ^1H NMR in CD_3COCD_3 of complex $[\text{Ir}_2\text{Ag}_2(\text{ppy})_4(\mu\text{-C}\equiv\text{CC}_6\text{H}_4\text{OMe-3})_4]$ (**2**)

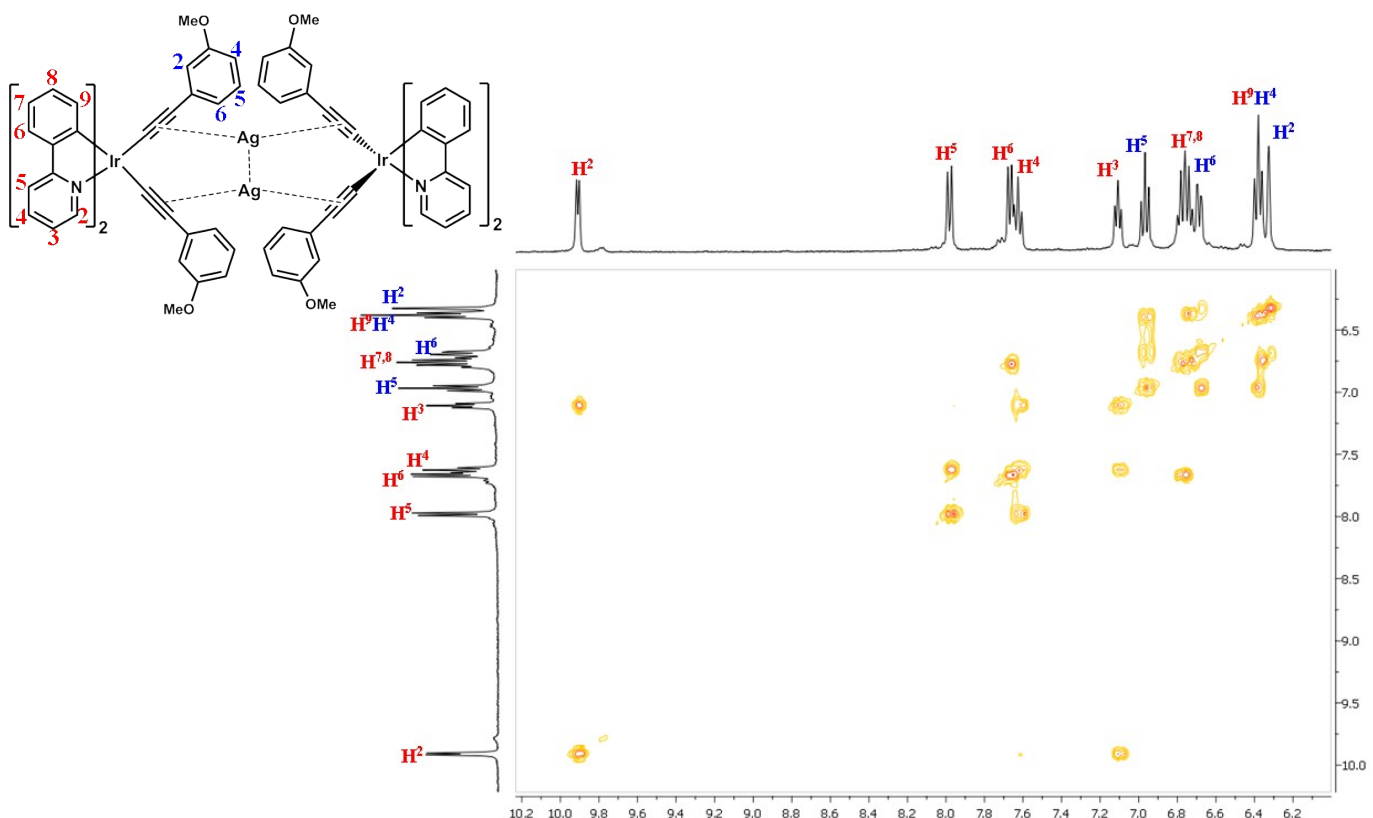


Fig. S7 Selected region of the ^1H - ^1H COSY in CD_3COCD_3 of complex $[\text{Ir}_2\text{Ag}_2(\text{ppy})_4(\mu\text{-C}\equiv\text{CC}_6\text{H}_4\text{OMe-3})_4]$ (**2**)

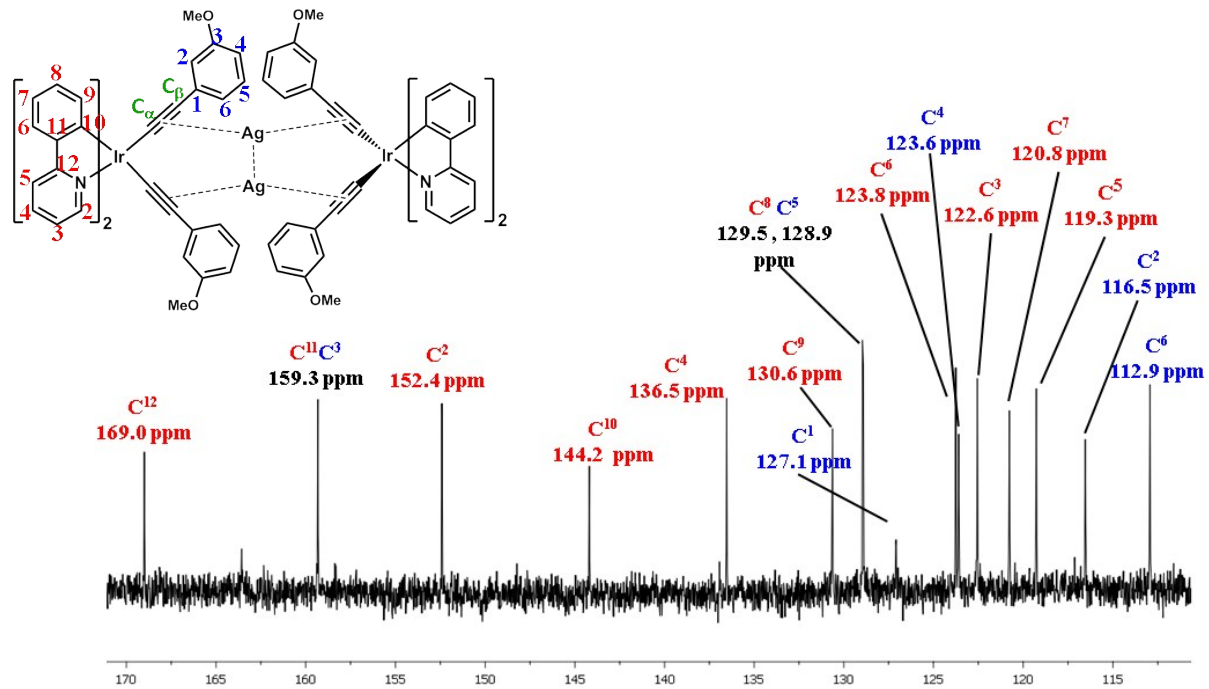


Fig. S8 Selected region of the $^{13}\text{C}\{^1\text{H}\}$ NMR in CD_3COCD_3 of complex $[\text{Ir}_2\text{Ag}_2(\text{ppy})_4(\mu\text{-C}\equiv\text{CC}_6\text{H}_4\text{OMe-3})_4]$ (**2**)

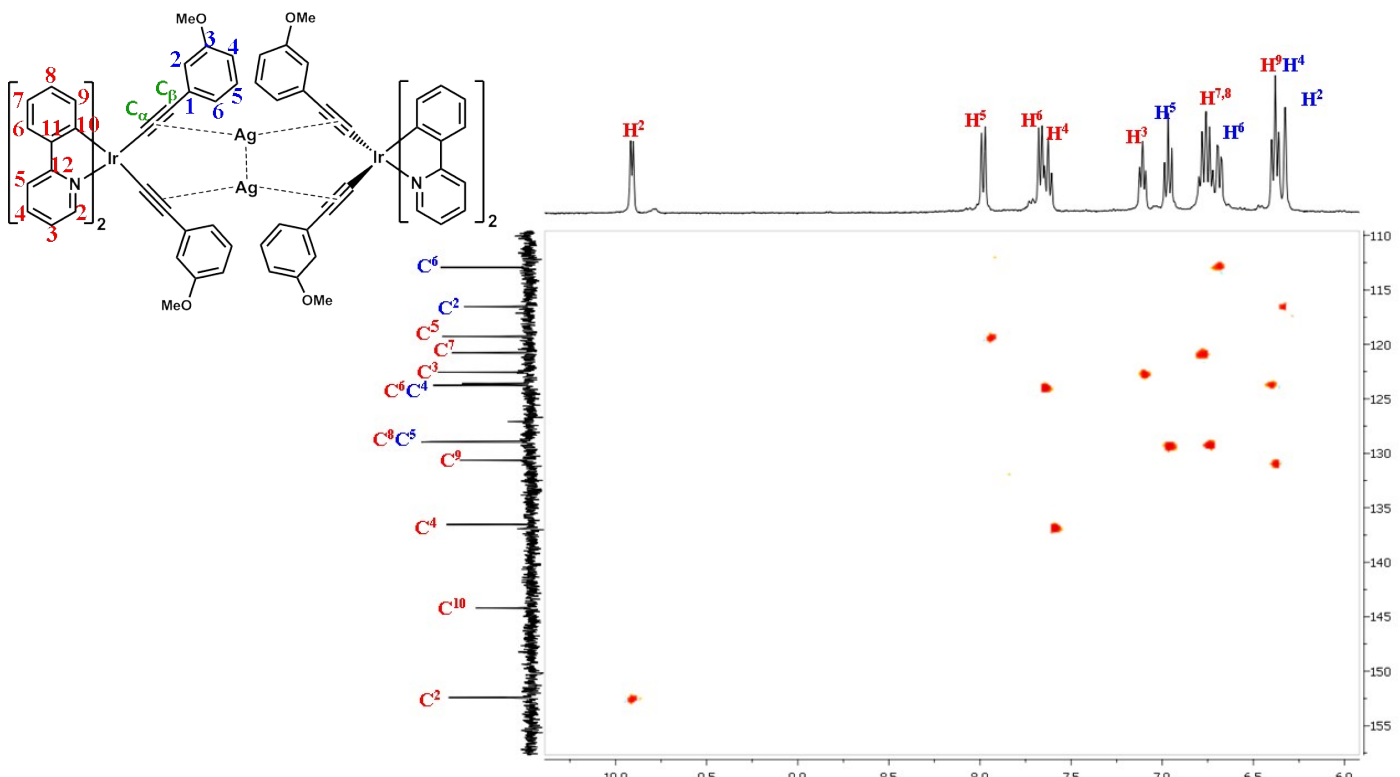


Fig. S9 Selected region of the HSQC in CD_3COCD_3 of complex $[\text{Ir}_2\text{Ag}_2(\text{ppy})_4(\mu\text{-C}\equiv\text{CC}_6\text{H}_4\text{OMe-3})_4]$ (**2**)

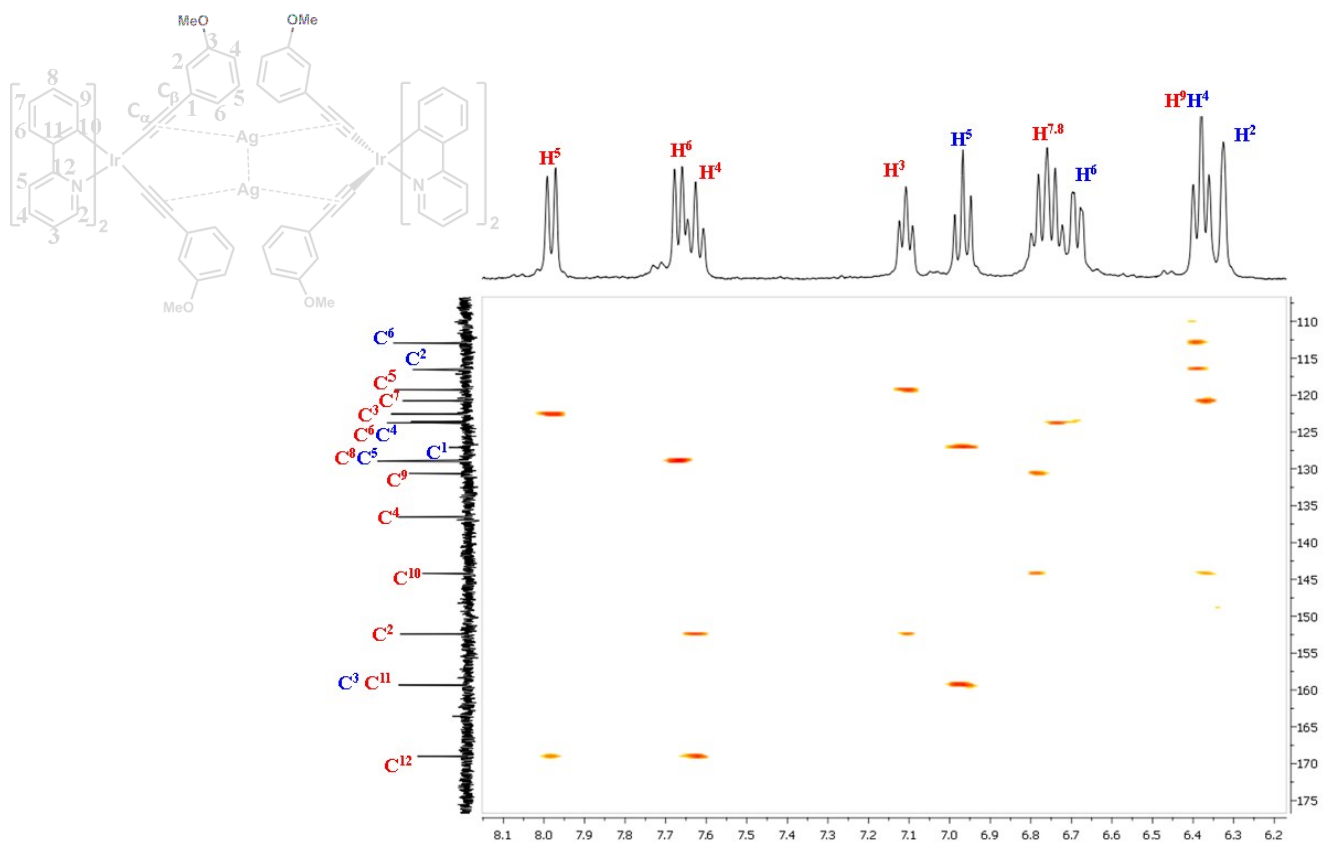


Fig. S10 Selected region of HMBC the in CD_3COCD_3 of complex $[\text{Ir}_2\text{Ag}_2(\text{ppy})_4(\mu-\text{C}\equiv\text{CC}_6\text{H}_4\text{OMe}-3)_4]$ (**2**)

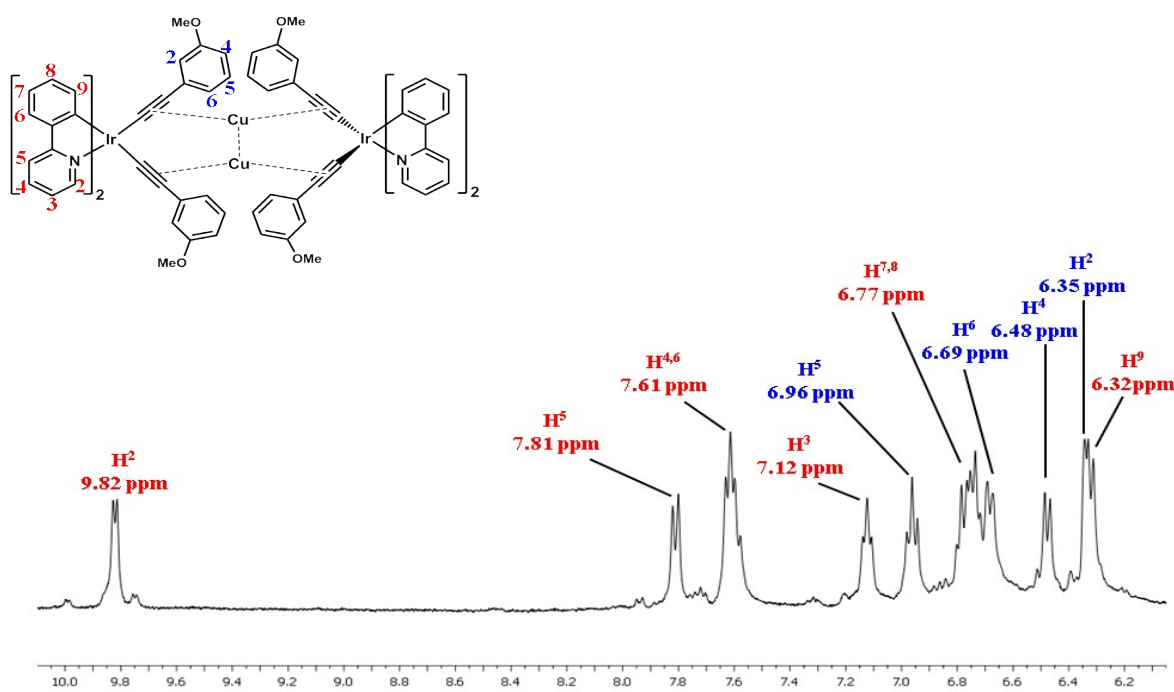


Fig. S11 Selected region of the ^1H NMR in CD_3COCD_3 of complex $[\text{Ir}_2\text{Cu}_2(\text{ppy})_4(\mu\text{-C}\equiv\text{CC}_6\text{H}_4\text{OMe-3})_4]$ (**3**)

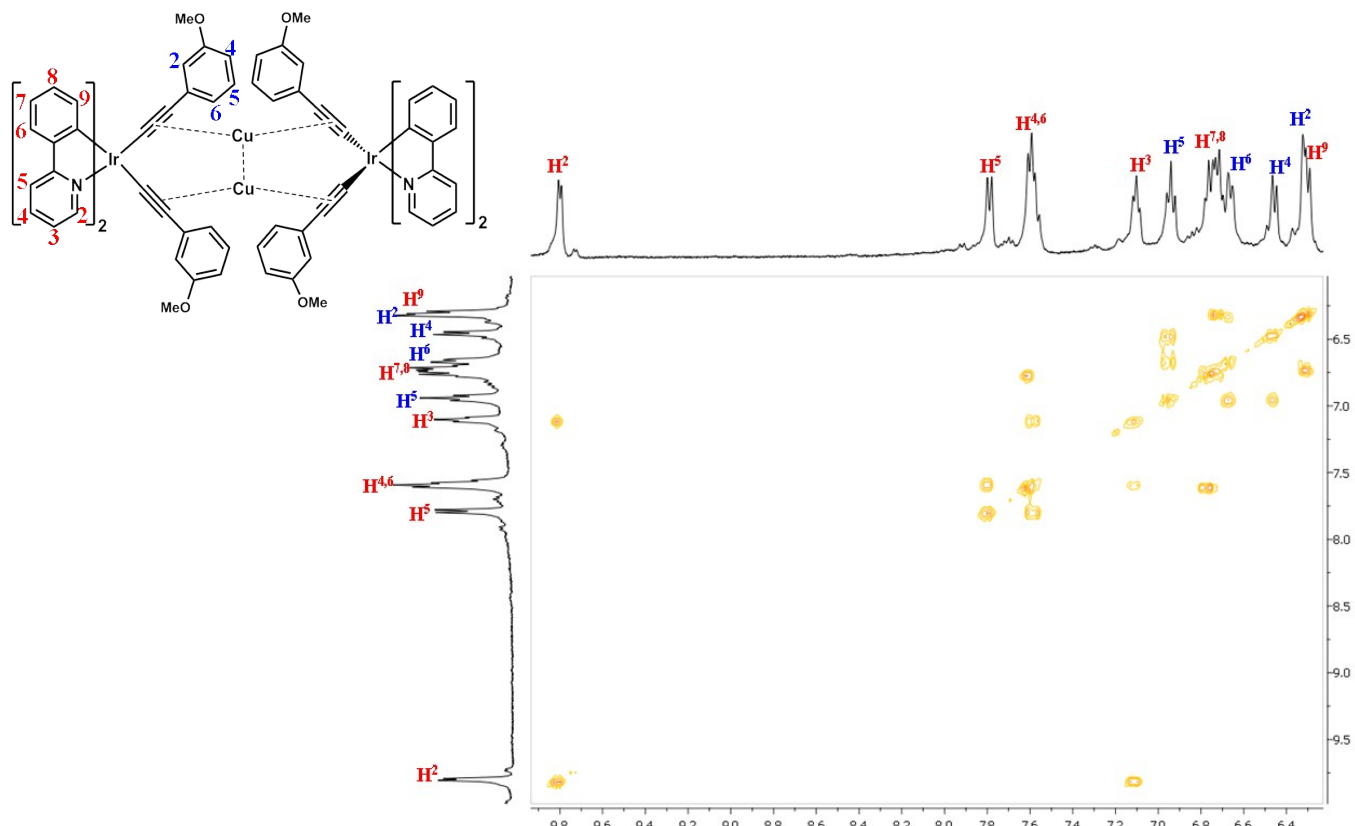


Fig. S12 Selected region of the ^1H - ^1H COSY in CD_3COCD_3 of complex $[\text{Ir}_2\text{Cu}_2(\text{ppy})_4(\mu\text{-C}\equiv\text{CC}_6\text{H}_4\text{OMe-3})_4]$ (**3**)

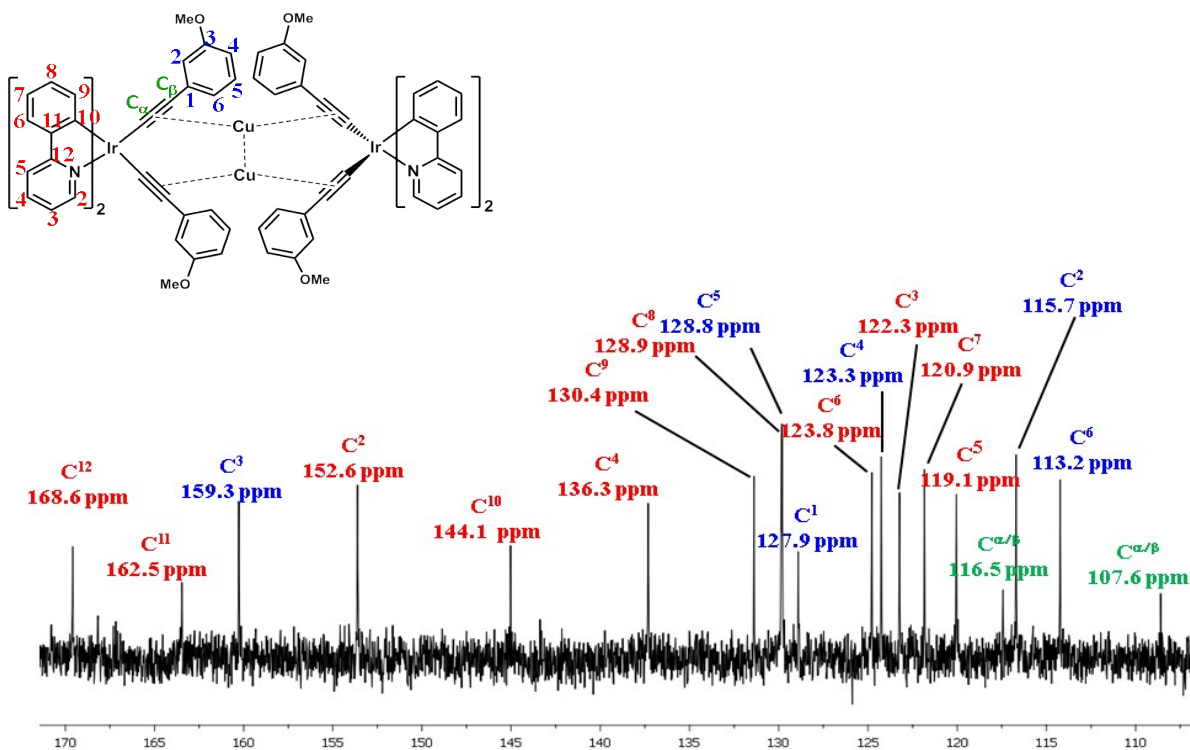


Fig. S13 Selected region of the ¹³C{¹H} NMR in CD₃COCD₃ of complex [Ir₂Cu₂(ppy)₄(μ-C≡CC₆H₄OMe-3)₄] (**3**)

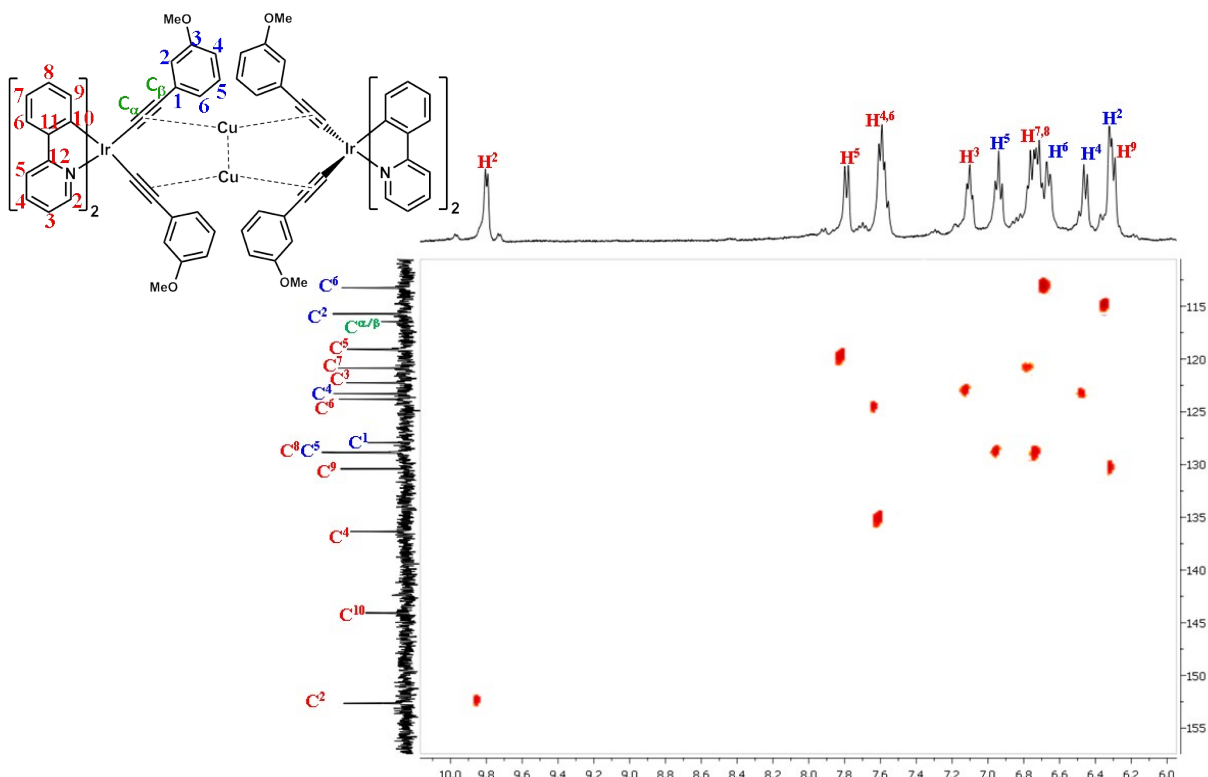


Fig. S14 Selected region of the HSQC in CD₃COCD₃ of complex [Ir₂Cu₂(ppy)₄(μ-C≡CC₆H₄OMe-3)₄] (**3**)

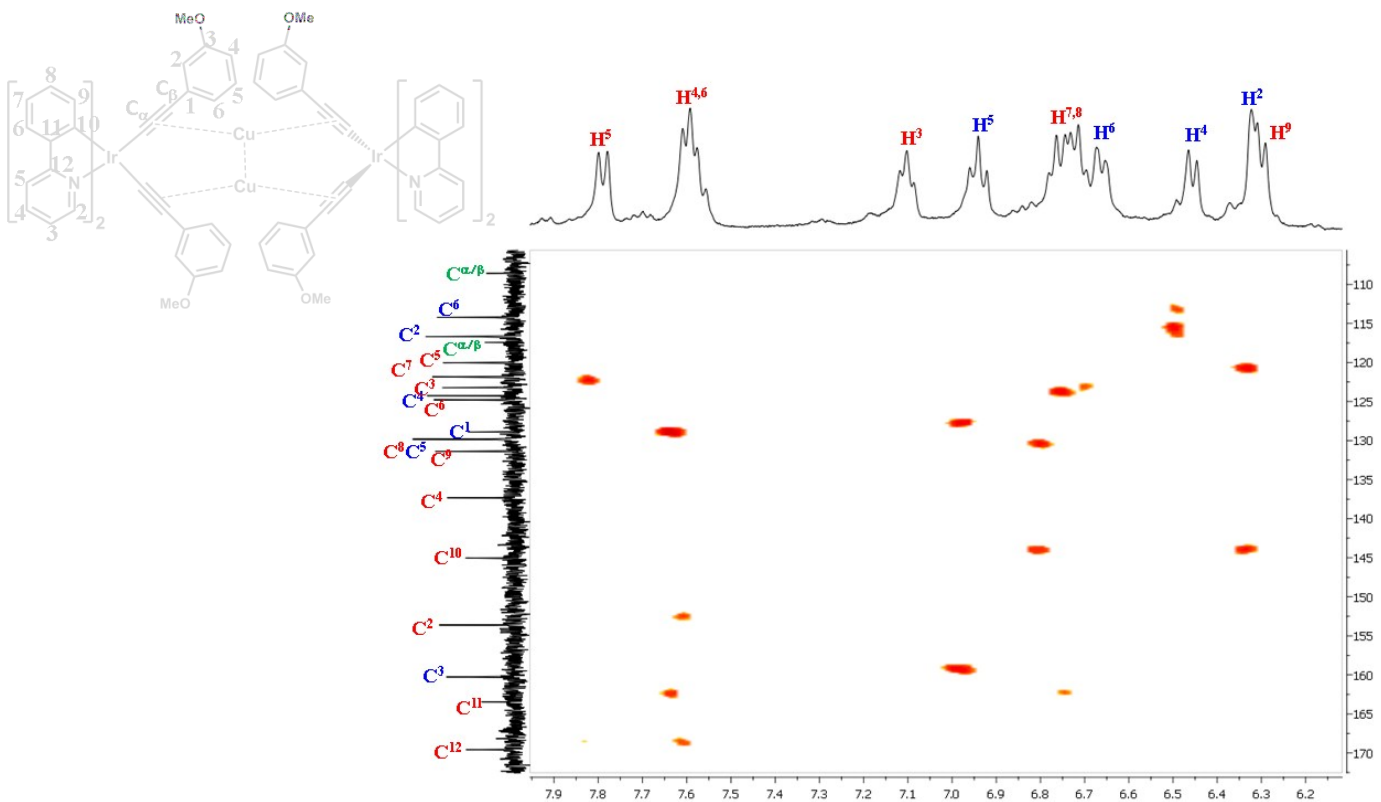
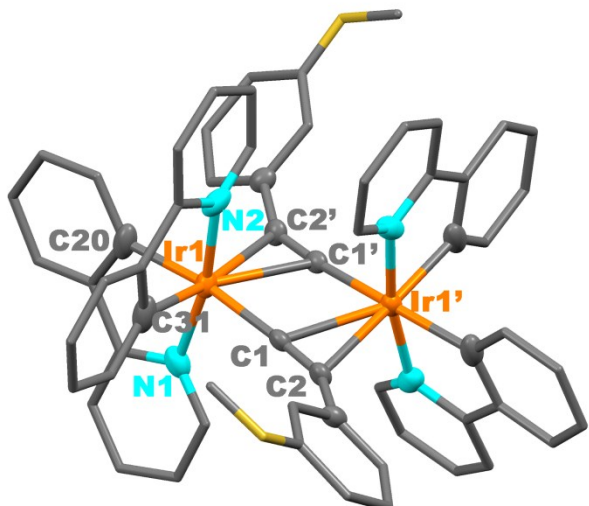


Fig. S15 Selected region of HMBC the in CD_3COCD_3 of complex $[\text{Ir}_2\text{Cu}_2(\text{ppy})_4(\mu-\text{CC}_6\text{H}_4\text{OMe}-3)_4]$ (3)

Table S1. X-ray Crystallographic Data for **1**·2CH₃COCH₃, **2**·2CH₂Cl₂ and **3**

	1 ·2CH ₃ COCH ₃	2 ·2CH ₂ Cl ₂	3
Empirical formula	C ₆₈ H ₅₈ Ir ₂ N ₄ O ₄	C ₈₂ H ₆₄ Ag ₂ Cl ₄ Ir ₂ N ₄ O ₄	C ₈₀ H ₆₀ Cu ₂ Ir ₂ N ₄ O ₄
F _w	1379.58	1826.38	1652.80
T (K)	220(2)	173(1)	173(1)
crystal system, space group	Orthorhombic, Fd2d	Triclinic, P-1	Tetragonal, I-4
a(Å)	14.8430(4)	15.1965(6)	17.5940(4)
b(Å)	26.4860(7)	15.8191(7)	17.5940(4)
c(Å)	27.9730(8)	17.1188(4)	21.0590(7)
α(deg)	90	68.885(2)	90
β(deg)	90	77.294(2)	90
γ(deg)	90	71.2650(10)	90
volume (Å ³)	10997.1(5)	3610.2(2)	6518.8(4)
Z	8	2	4
D _{calcd} (Mg/m ³)	1.667	1.680	1.684
absorption coefficient (mm ⁻¹)	4.891	4.259	4.769
F(000)	5440	1780	3248
θ range for data collection (deg)	3.107 to 27.477	2.469 to 27.342	3.606 to 27.425
no of data / restraints / params	6268 / 1 / 353	16153 / 0 / 860	7402 / 422 / 436
goodness-of-fit on F ² ^[a]	1.029	1.031	1.041
final R indices [I>2σ(I)] ^[a]	R1 = 0.0243, wR2 = 0.0483	R1 = 0.0446, wR2 = 0.1054	R1 = 0.0389, wR2 = 0.0784
R indices (all data) ^[a]	R1 = 0.0311, wR2 = 0.0503	R1 = 0.0684, wR2 = 0.1134	R1 = 0.0552, wR2 = 0.0839
largest diff peak and hole (e.Å ⁻³)	0.812 and -0.745	1.863 and -1.972	2.535 and -0.921

^[a] $R1 = \sum(|F_o| - |F_c|)/\sum|F_o|$; $wR2 = [\sum w(F_o^2 - F_c^2)^2/\sum wF_o^2]^{1/2}$; goodness of fit = $\{\sum[w(F_o^2 - F_c^2)^2]/(N_{\text{obs}} - N_{\text{param}})\}^{1/2}$; $w = [\sigma^2(F_o) + (g_1P)^2 + g_2P]^{-1}$; $P = [\max(F_o^2; 0 + 2F_c^2)]/3$.



1·2CH₃COCH₃ (only shown the ΔΔ form)

The structural features of **1** are comparable to those reported for the related tolyl acetylidyne derivative ¹-Fig. S16 and Table S2-. Thus, the Ir-C(ppy) bond lengths and Ir-C_α and Ir-C_β distances within the central dimetallacycle Ir₂(C≡C)₂ are almost identical to those of [Ir₂(ppy)₄(μ-C≡CTol)₂]¹. The observed slightly larger Ir···Ir separation (3.6896(6) **1** vs. 3.669(1) Å in [Ir₂(ppy)₄(μ-C≡CTol)₂]) and the smaller puckering at the central Ir₂(C≡C)₂ core [dihedral angle at the C_α···C_{α'} line 169.06° in **1** vs. 169.2° in [Ir₂(ppy)₄(μ-C≡CTol)₂]] can be attributed to the more steric bulkiness of the methoxy units at the *meta* position.

¹ J. Fernández-Cestau, N. Giménez, E. Lalinde, P. Montaño, M. T. Moreno and S. Sánchez, *Organometallics*, 2015, **34**, 1766

Fig. S16
Two different views of the X-ray crystal structure of

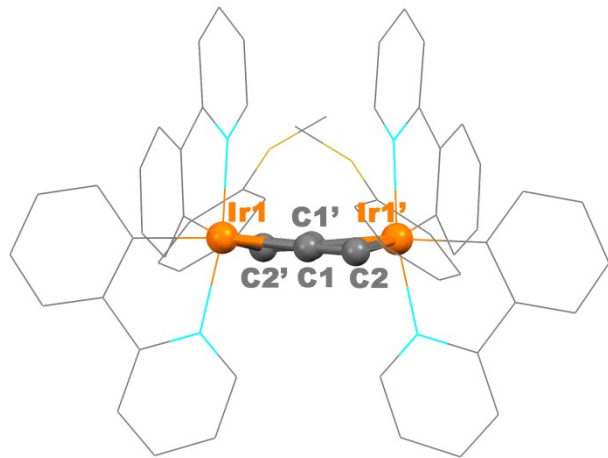


Table S2. Selected Bond Lengths (Å) and Angles (°) of **1·2CH₃COCH₃**

Distances [Å]			
Ir1-C1	2.061(6)	Ir1-N1	2.051(6)
C1-C2	1.227(8)	Ir1-N2	2.069(7)
C2-C3	1.458(8)	Ir1-C20	2.045(6)
Ir1-C1'	2.414(5)	Ir1-C31	2.033(6)
Ir1-C2'	2.387(5)	Ir1-Ir1'	3.6891(6)

Angles [°]			
Ir1-C1-C2	174.6(5)	C2'-Ir1-C31	171.5(3)
C1-C2-C3	148.5(6)	C2'-Ir1-N2	91.8(2)
C1-Ir1-C2'	97.8(2)	N1-Ir1-C20	79.4(5)
C1-Ir1-N1	93.7(3)	N1-Ir1-C31	93.6(3)
C1-Ir1-C20	171.7(4)	N1-Ir1-N2	169.6(3)
C1-Ir1-C31	86.2(2)	N2-Ir1-C31	80.3(3)
C1-Ir1-N2	94.3(3)	N2-Ir1-C20	92.1(5)
C2'-Ir1-N1	93.6(2)	C20-Ir1-C31	89.7(3)
C2'-Ir1-C20	87.3(2)		

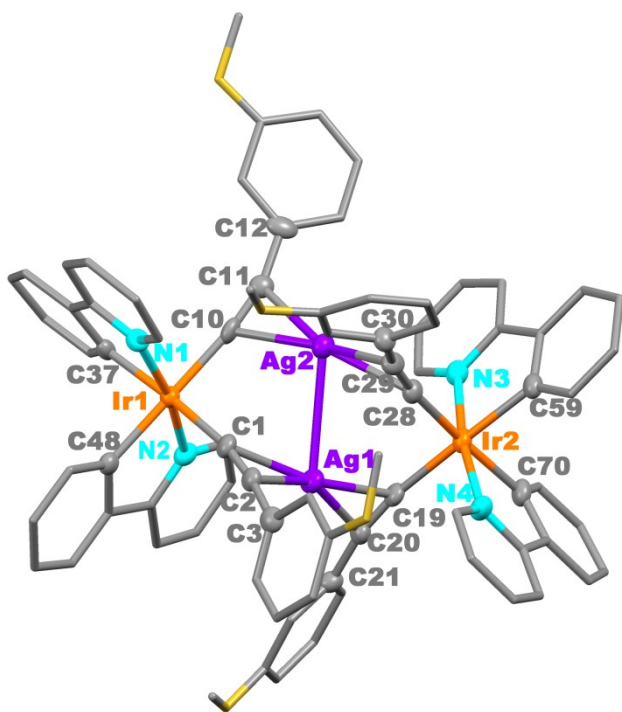


Fig. S17 X-ray crystal structure of $\mathbf{2}\cdot\text{2CH}_2\text{Cl}_2$

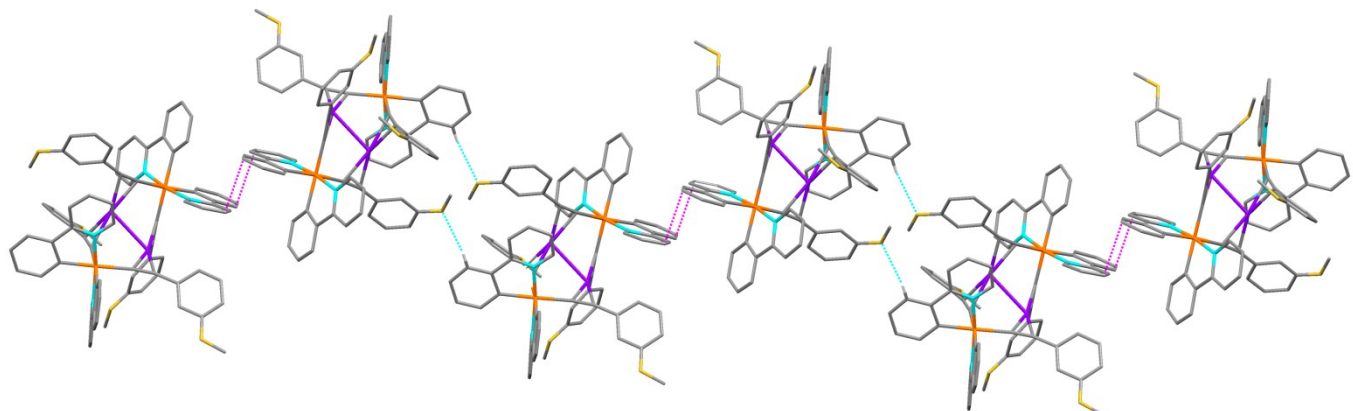


Fig. S18 Crystal packing of complex $[\text{Ir}_2\text{Ag}_2(\text{ppy})_4(\text{C}\equiv\text{C}(\text{C}_6\text{H}_4\text{OMe}-3)_4)] \cdot 2\cdot\text{2CH}_2\text{Cl}_2$ (minimum $\pi\cdots\pi$ interactions 3.370 \AA forming dimers, pink). The dimers are packing through secondary weak interactions (blue) [$\text{O}_{\text{OMe}}\cdots\text{H}_{\text{ppy}}$ 2.670 \AA].

Table S3. Selected Bond Lengths (Å) and Angles (°) of **2**·2CH₂Cl₂

Distances [Å]			
Ir1-C1	2.082(6)	Ir2-C28	2.065(6)
C1-C2	1.213(8)	C28-C29	1.234(8)
C2-C3	1.467(8)	C29-C30	1.456(8)
Ir1-C10	2.051(6)	Ir2-N3	2.058(5)
C10-C11	1.241(8)	Ir2-N4	2.073(5)
C11-C12	1.449(8)	Ir2-C59	2.068(6)
Ir1-N1	2.062(4)	Ir2-C70	2.065(6)
Ir1-N2	2.055(4)	Ag2-C10	2.288(5)
Ir1-C37	2.041(5)	Ag2-C28	2.305(6)
Ir1-C48	2.037(6)	Ag2-C11	2.292(6)
Ag1-C1	2.302(6)	Ag2-C29	2.287(6)
Ag1-C2	2.283(5)	Ir1-Ag1	3.6603(6)
Ag1-C19	2.233(5)	Ir1-Ag2	3.5937(7)
Ag1-C20	2.324(6)	Ir2-Ag1	3.4654(7)
Ir2-C19	2.075(6)	Ir2-Ag2	3.7806(6)
C19-C20	1.216(8)	Ag1-Ag2	2.9985(7)
C20-C21	1.448(8)	Ir1-Ir2	6.5373(6)
Angles [°]			
Ir1-C1-C2	169.2(5)	Ir2-C19-C20	171.6(5)
C1-C2-C3	171.4(6)	C19-C20-C21	168.5(6)
C1-Ir1-N1	95.1(2)	C19-Ir2-N3	96.7(2)
C1-Ir1-N2	92.5(2)	C19-Ir2-N4	89.2(2)
C1-Ir1-C48	84.4(2)	C19-Ir2-C70	85.9(2)
C1-Ir1-C10	97.5(2)	C19-Ir2-C28	99.7(2)
Ir1-C10-C11	172.6(5)	Ir2-C28-C29	166.4(5)
C10-C11-C12	164.4(6)	C28-C29-C30	163.5(6)
C10-Ir1-N1	88.6(2)	C28-Ir2-N3	92.5(2)
C10-Ir1-N2	97.7(2)	C28-Ir2-N4	92.9(2)
C10-Ir1-C37	87.4(2)	C28-Ir2-C59	84.7(2)
N1-Ir1-C37	79.7(2)	N3-Ir2-C59	79.6(2)
N2-Ir1-C48	79.4(2)	N4-Ir2-C70	79.3(2)
N1-Ir1-C48	94.0(2)	N3-Ir2-C70	94.6(2)
N2-Ir1-C37	92.1(2)	N4-Ir2-C59	94.0(2)
C37-Ir1-C48	91.0(2)	C59-Ir2-C70	90.2(2)
N1-Ir1-N2	169.46(19)	N3-Ir2-N4	171.21(19)
C1-Ag1-C2	30.67(19)	C10-Ag2-C11	31.4(2)
C19-Ag1-C20	30.9(2)	C28-Ag2-C29	31.2(2)
C1-Ag1-C19	166.7(2)	C10-Ag2-C28	161.7(2)
C2-Ag1-C20	151.5(2)	C11-Ag2-C29	154.2(2)

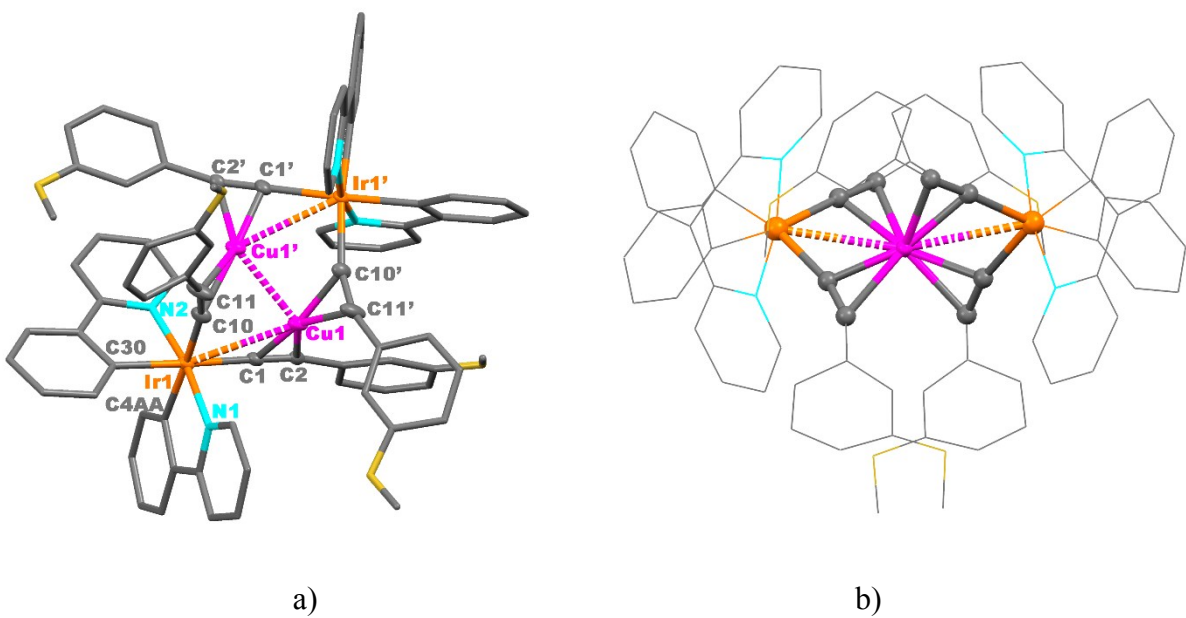


Fig. S19 Two different views of the X-ray crystal structure of **3**

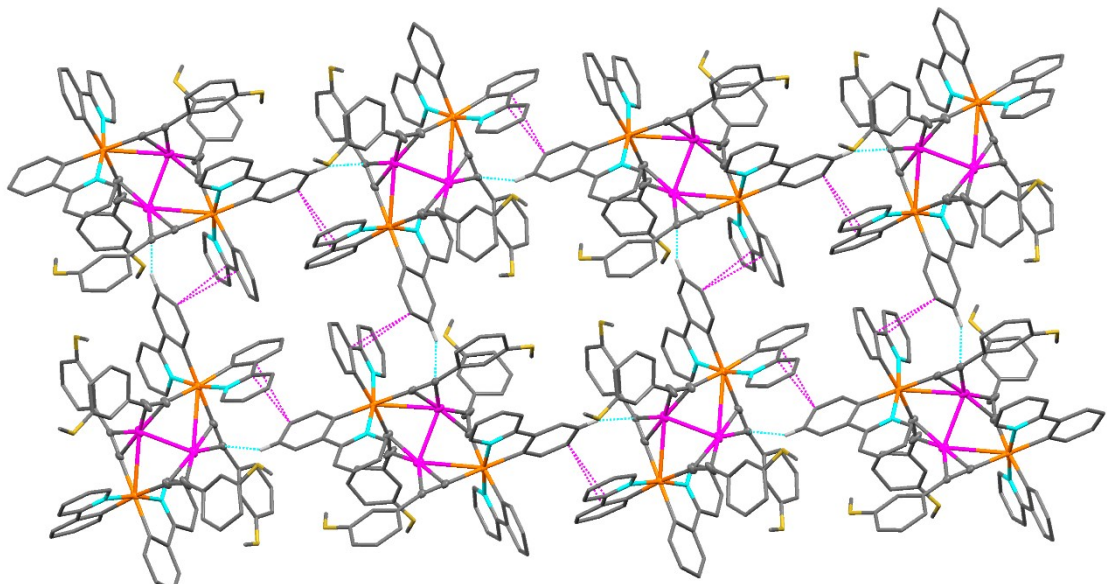


Fig. S20 Crystal packing of complex $[\text{Ir}_2\text{Cu}_2(\text{ppy})_4(\text{C}\equiv\text{C}(\text{C}_6\text{H}_4\text{OMe}-3)_4)]$ (**3**) [minimum $\pi\cdots\pi$ interactions (pink) 3.299 Å and secondary weak interactions (blue) $\text{H}_{\text{ppy}}\cdots\text{C}_\beta$ 2.672 Å].

Table S4. Selected Bond Lengths (\AA) and Angles ($^{\circ}$) of **3**

Distances [\AA]			
Ir1-C1	2.080(10)	Ir1-C30	2.077(9)
C1-C2	1.220(13)	Cu1-C1	1.991(10)
C2-C3	1.445(15)	Cu1-C2	2.102(10)
Ir1-C10	2.086(10)	Cu1'-C10	2.032(9)
C10-C11	1.212(15)	Cu1'-C11	2.062(12)
C11-C12A ^a	1.487(15)	Cu1-Cu1'	2.732(2)
Ir1-N1	2.066(8)	Ir1-Cu1	3.154(1)
Ir1-N2	2.047(8)	Ir1-Cu1'	3.529(1)
Ir1-C4AA	2.063(9)	Ir1-Ir1'	6.0202(5)
Angles [$^{\circ}$]			
Ir1-C1-C2	178.1(9)	N1-Ir1-C4AA	79.7(3)
C1-C2-C3	167.2(10)	N2-Ir1-C30	80.0(3)
C1-Ir1-N1	91.8(3)	N1-Ir1-C30	93.2(3)
C1-Ir1-N2	94.5(3)	N2-Ir1-C4AA	93.2(3)
C1-Ir1-C4AA	88.0(3)	C4AA-Ir1-C30	88.2(3)
C1-Ir1-C10	99.5(4)	N1-Ir1-N2	170.4(3)
Ir1-C10-C11	166.1(10)	C1-Cu1-C2	34.6(4)
C10-C11-C12A ^a	158.4(13)	C10-Cu1'-C11	34.4(4)
C10-Ir1-N1	92.9(4)	C1-Cu1-C10'	163.2(4)
C10-Ir1-N2	93.2(4)	C2-Cu1-C11'	136.8(5)
C10-Ir1-C30	85.0(4)	Cu1-Ir1-Cu1'	47.86(3)

^a Relative to the majority component of the disordered methoxyphenyl ring (See Experimental)

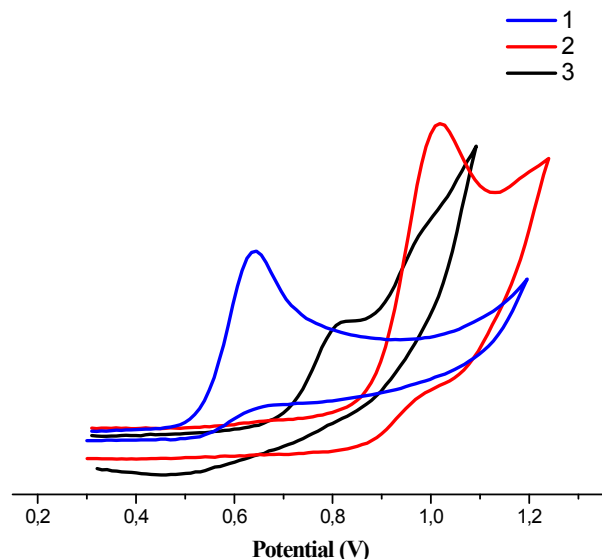


Fig. S21a Cyclic voltammogram of **1-3** in 0.1 M NBu₄PF₆/THF at a scan rate of 100 mVs⁻¹.

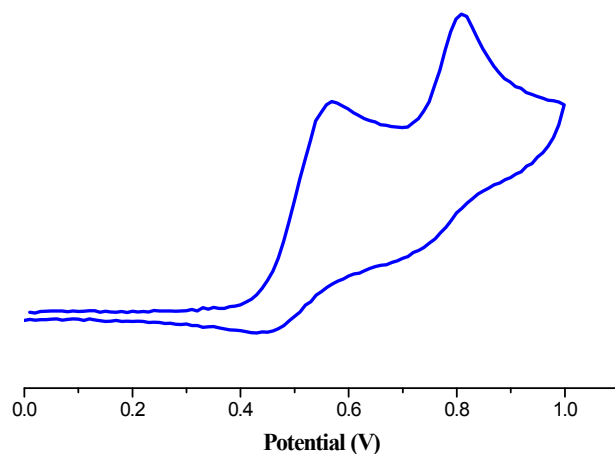


Fig. S21b Cyclic voltammogram of **1** in 0.1 M NBu₄PF₆/CH₂Cl₂ at a scan rate of 100 mVs⁻¹.

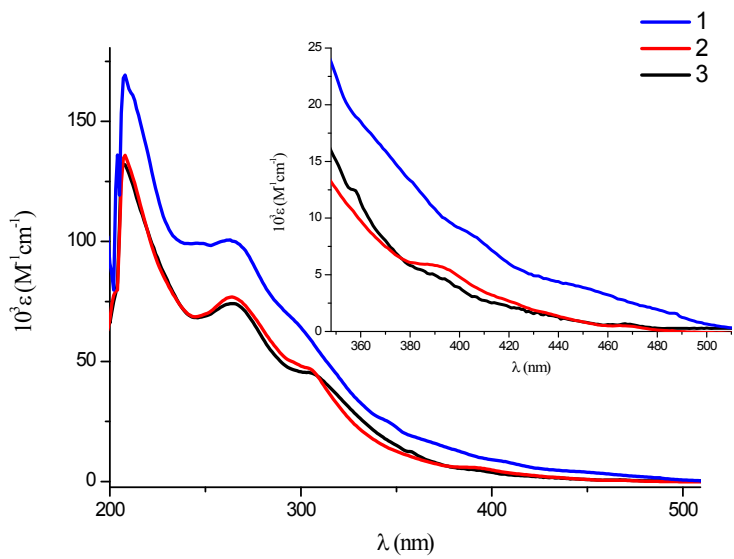
Table S5. Absorption data (solid state and solution 10⁻⁴ M, 298 K) and Electrochemical Data ^a (THF 10⁻⁴ M)

	λ (nm)(10 ³ ϵ M ⁻¹ cm ⁻¹)	$E_{(ox)}^b$ (V)
1	208(169), 246(99.3), 262(100.6), 296(67.5), 345(25.2), 367(16.7), 406(8.4), 452(3.7), 487(1.6) THF	0.65 0.57, 0.81 ^c
2	216, 260, 322, 355, 370, 400, 415, 467 solid 208(136), 264(77.1), 304(47.5), 392(6.0), 433(2.0), 468(0.8) THF 221(180), 267(145.8), 304(92.0), 394(13.4), 433(6.1), 464(2.9) CH₂Cl₂	0.94
3	226, 271, 294, 314, 368, 400, 436, 469 solid 207(132), 264(74.1), 305(45.3), 358(12.4), 392(4.7), 427(1.7), 469(0.7) THF 221(131), 266(112), 304(71.6), 354(20.8), 392(13.5), 433(6.1), 464(3.7) CH₂Cl₂	0.82, 0.98

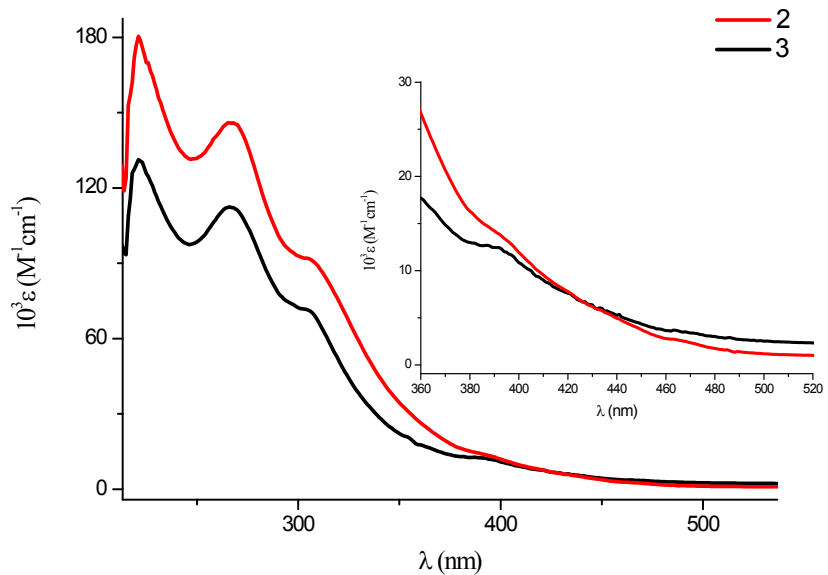
^a Using 0.1M NBu₄PF₆ as electrolyte, scan rate 100 mVs⁻¹ and vs Ag/AgCl reference electrode.

^b Peak potentials, E_{pa}, for irreversible processes.

^c CH₂Cl₂



a)



b)

Fig. S22 UV-visible absorption spectra at 298 K of a) **1-3** in THF (10^{-4} M) b) **2, 3** in CH_2Cl_2 (10^{-4} M).

Table S6. Photophysical data for complexes in solid state, in THF (1×10^{-4} M) and in CH_2Cl_2 (1×10^{-4} M) at 298 and 77 K.

		T/K	$\lambda_{\text{em}}(\lambda_{\text{ex}})/\text{nm}$	$\tau/\mu\text{s}^a$	ϕ^b	$K_r(\text{s}^{-1})^c$	$K_{nr}(\text{s}^{-1})^d$
1	THF	298	525,550 (410-470)	0.7	0.00 6	8.5×10^3	3.1×10^6
		77	520,545 (365-470)	15.9			
	10% in PMMA	298	530 (365-430)	0.4	0.00 9	2.3×10^4	2.5×10^6
2	Solid state	298	515, 540 (400-430)	0.3	0.07	2.3×10^5	3.1×10^6
		77	505,530 (365-430)	14.6(88%),60.7(12%)			
	THF	298	511,540 (365-430)	1.1	0.01 8	1.6×10^4	8.9×10^5
		77	475, 505, 535 (365-430)	9.6			
	CH ₂ Cl ₂	298	480, 505 (365-430)	0.02	0.01	5×10^5	4.9×10^7
		77	475,505,545 (390-430)	9.4			
	10% in PMMA	298	487, 507 (365-430)	1.3	0.23	1.8×10^5	5.9×10^5
3	Solid state	298	615 (420-500)	6.1	0.18	2.9×10^4	1.3×10^5
		77	605 (390-480)	24.4(61%),6.5(39%)			
	THF	298	625 (390-430)	1.0	0.01 8	1.8×10^4	9.8×10^5
		77	520, 550 (365-450)	42.3			
	CH ₂ Cl ₂	298	620 (390-480)	0.9	0.01	1.1×10^4	1.1×10^6
		77	595 (420-480)	32.7			
	10% in PMMA	298	600 (365-490)	22.1	0.07	3.2×10^3	4.2×10^4

^a Measured in the λ_{max}

^b Absolute quantum yields determined by the absolute method using an integrated sphere

^c Radiative rate constant $K_r = \phi/\tau$

^d Nonradiative rate constant $K_{nr} = (1-\phi)/\tau$

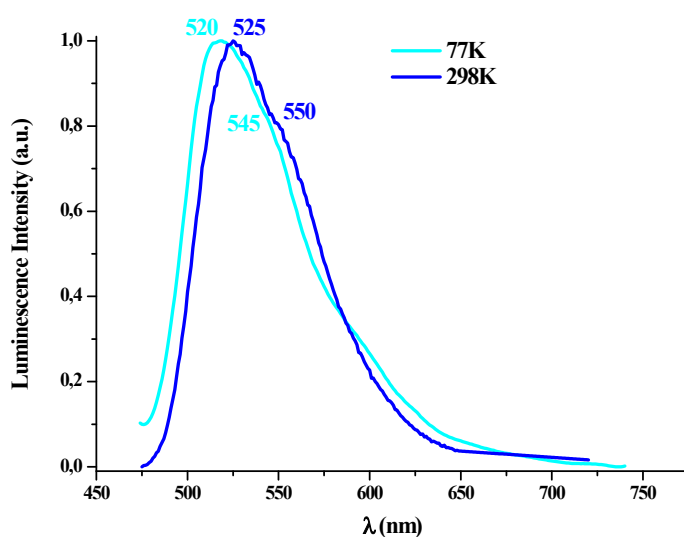


Fig. S23 Normalized emission spectra in THF (10^{-4} M) at 298 and 77 K of **1**

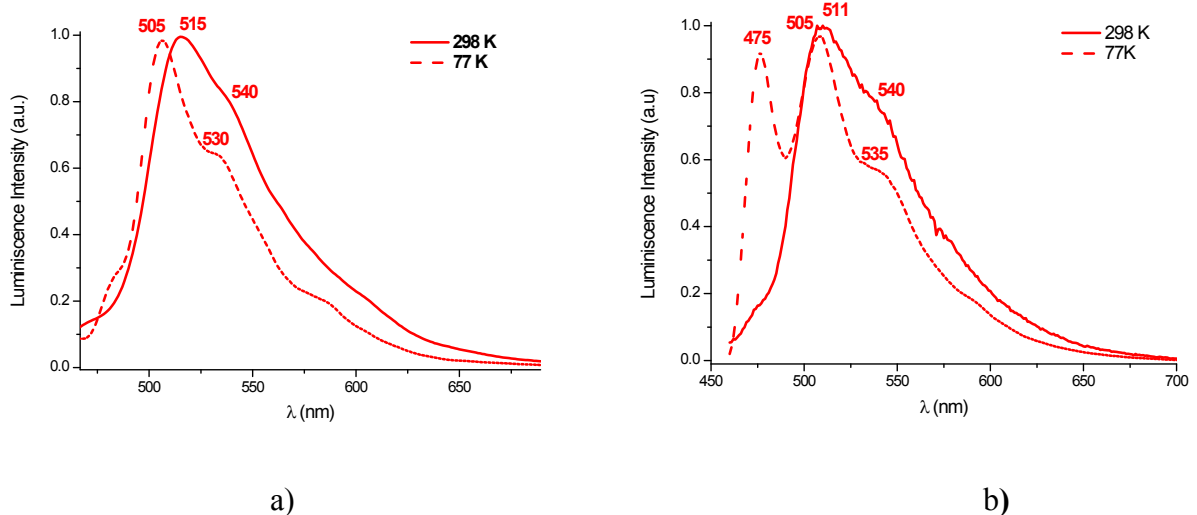


Fig. S24 Normalized emission spectra of **2** a) in solid state b) in THF (10^{-4} M) at 298K and 77 K

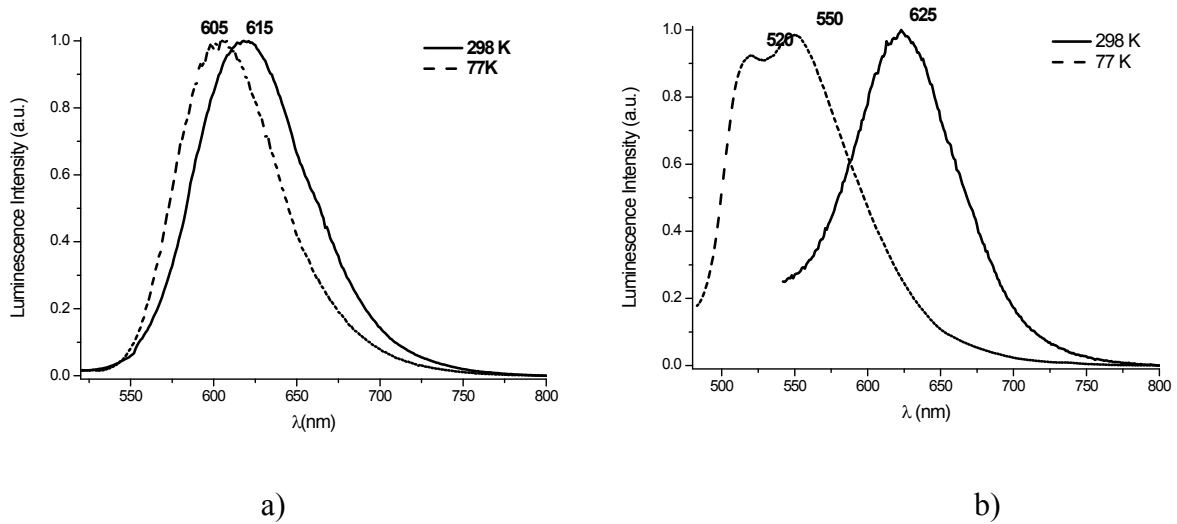


Fig. S25 Normalized emission spectra of **3** a) in solid state b) in THF (10^{-4} M) at 298K and 77 K

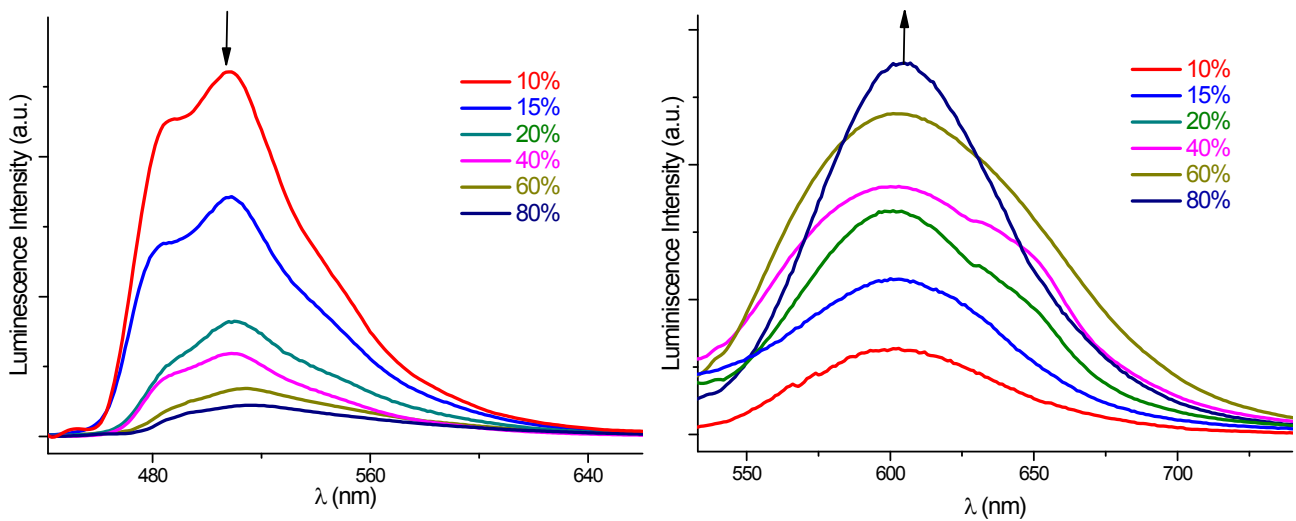


Fig. S26 Emission spectra of **2** ($\phi = 0.23\text{-}0.01$) and **3** ($\phi = 0.07\text{-}0.14$) in PMMA thin films at variable concentrations (wt%) at 298 K.

Table S7. DFT optimized geometries for ground state and triplet state of complex 2.

	X-ray	S ₀	T ₁
Distances [Å]			
Ir1-Ag2	3.5937(7)	3.742	3.752
Ir1-Ag1	3.6603(6)	3.782	3.767
Ir2-Ag1	3.4654(7)	3.366	3.363
Ir2-Ag2	3.7806(6)	3.838	3.846
Ir1-C1	2.082(6)	2.048	2.073
Ir1-C10	2.051(6)	2.063	2.062
Ir2-C19	2.075(6)	2.077	2.082
Ir2-C28	2.065(6)	2.081	2.077
C1-C2	1.213(8)	1.241	1.241
C10-C11	1.241(8)	1.250	1.248
C19-C20	1.216(8)	1.246	1.239
C28-C29	1.234(8)	1.240	1.246
Ag1-C1	2.302(6)	2.398	2.397
Ag2-C10	2.288(5)	2.309	2.308
Ag1-C19	2.233(5)	2.364	2.355
Ag2-C28	2.305(6)	2.400	2.401
Ag1-C2	2.283(5)	2.364	2.368
Ag2-C11	2.292(6)	2.434	2.434
Ag1-C20	2.324(6)	2.268	2.282
Ag2-C29	2.287(6)	2.311	2.311
Ag1-Ag2	2.9985(7)	3.103	3.095
Ir1-Ir2	6.5373(6)	6.527	6.536
Angles[Å]			
Ir1-C1-C2	169.2(5)	172.33	171.75
Ir2-C19-C20	171.6(5)	171.84	171.42
Ir1-C10-C11	172.6(5)	169.41	168.99
Ir2-C28-C29	166.4(5)	177.31	177.10
C1-C2-C3	168.5(6)	171.88	172.28
C19-C20-C21	168.2(7)	158.13	159.81
C10-C11-C12	164.4(6)	166.51	166.72
C28-C29-C30	163.5(6)	176.65	176.13

Table S8. DFT optimized geometries for ground state and triplet state of complex **3**.

	X-ray	S_0	T_1
Distances [Å]			
Ir1-Cu1	3.154(1)	2.928	3.078
Ir1'-Cu1'	3.529(1)	3.653	3.707
Ir1'-Cu1	3.529(1)	3.651	3.575
Ir1'-Cu1'	3.154(1)	2.928	2.725
Ir1-C1	2.080(10)	2.083	2.079
Ir1-C10	2.086(10)	2.085	2.069
Ir1'-C1'	2.08(1)	2.083	2.083
Ir1'-C10'	2.09(1)	2.088	2.081
C1-C2	1.220(13)	1.240	1.241
C10-C11	1.212(15)	1.245	1.244
C1'-C2'	1.220(13)	1.240	1.239
C10'-C11'	1.212(15)	1.245	1.304
Cu1-C1	1.991(10)	2.004	2.008
Cu1-C10'	2.032(9)	2.134	1.996
Cu1'-C10	2.032(9)	2.134	2.211
Cu1'-C1'	1.991(10)	2.004	2.069
Cu1-C2	2.102(10)	2.227	2.182
Cu1-C11'	2.062(12)	2.127	2.423
Cu1'-C11	2.062(12)	2.127	2.188
Cu1'-C2'	2.102(10)	2.226	2.315
Cu1-Cu1'	2.732(2)	2.692	2.520
Ir1-Ir1'	6.0202(5)	5.943	6.025
Angles[Å]			
Ir1-C1-C2	178.1(9)	173.55	176.26
Ir1-C10-C11	166.1(10)	162.20	166.96
Ir1'-C1'-C2'	178.1(9)	173.35	166.83
Ir1'-C10'-C11'	166.1(10)	162.14	143.11
C1-C2-C3	167.2(10)	177.3	177.11
C10-C11-C12A ^a	158.4(13)	162.47	169.18
C1'-C2'-C3'	167.2(10)	176.98	174.82
C10'-C11'-C12A ^a	158.4(13)	162.66	171.64

^a Relative to the majority component of the disordered methoxyphenyl ring (See Experimental)

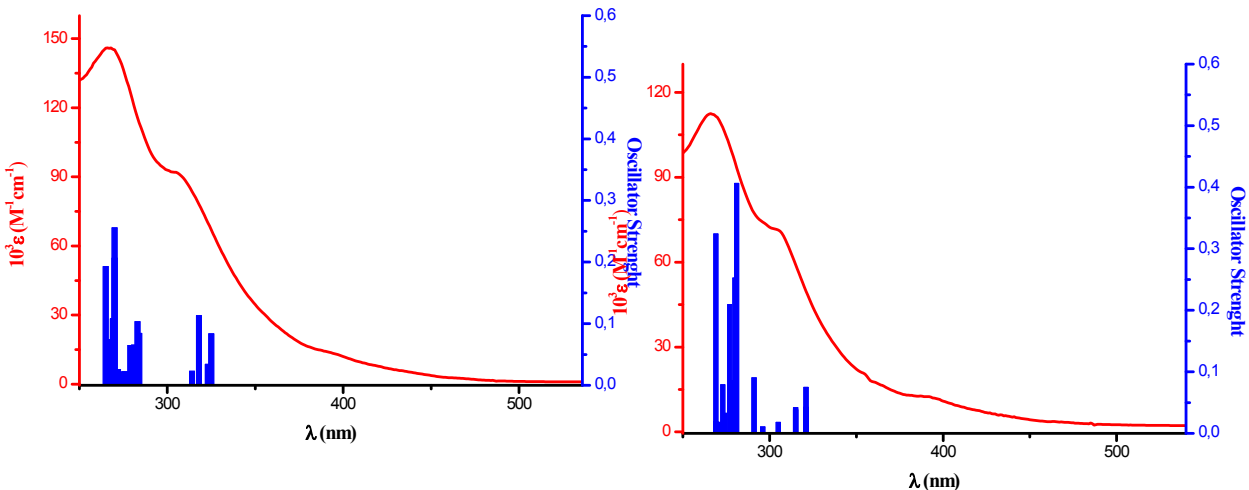


Fig. S27 Calculated absorptions bars in CH_2Cl_2 and the low energy section of experimental UV-vis in CH_2Cl_2 ($1 \times 10^{-4} \text{ M}$) at 298 K for **2** (left) and **3** (right).

Table S9. Composition of Frontier Molecular Orbitals (%) in Terms of Ligands and Metals in the Ground-State for **2** and **3**.

2	eV	Ag(1)	Ag(2)	Ir(1)	C≡C(C ₆ H ₄ OMe-3)(Ir1)	ppy(Ir1)	Ir(2)	C≡C(C ₆ H ₄ OMe-3)(Ir2)	ppy(Ir2)
L+8	1.22	3	1	1	26	2	0	6	61
L+7	1.18	1	2	2	20	59	0	4	12
L+6	1.09	3	4	1	14	15	2	2	58
L+5	0.96	2	4	0	4	12	3	56	18
L+4	0.74	10	8	0	17	17	0	23	25
L+3	0.68	1	0	2	1	88	0	2	6
L+2	0.65	1	0	0	1	4	2	2	89
L+1	0.6	0	1	2	3	92	0	1	1
LUMO	0.51	0	1	0	1	1	2	4	91
HOMO	-6.82	2	0	1	3	0	40	14	40
H-1	-6.91	1	1	38	11	46	1	2	0
H-2	-7.17	2	0	1	2	2	25	61	8
H-3	-7.25	4	0	30	42	11	2	5	6
H-4	-7.3	0	2	34	43	19	0	0	1
H-5	-7.5	1	1	1	2	5	8	10	73
H-6	-7.53	0	0	4	9	79	1	3	5
H-7	-7.58	0	3	0	1	1	36	26	33
H-8	-7.77	1	1	4	8	36	5	32	13

3	eV	Cu(1)	Cu(2)	Ir(1)	C≡C(C ₆ H ₄ OMe-3)(Ir1)	ppy(Ir1)	Ir(2)	C≡C(C ₆ H ₄ OMe-3)(Ir2)	ppy(Ir2)
L+8	1.21	1	1	1	20	30	1	18	28
L+7	1.17	2	2	1	42	3	1	45	4
L+6	1.06	1	3	1	21	6	2	26	39
L+5	1.06	3	1	1	11	55	1	5	22
L+4	0.84	9	9	0	7	34	0	7	33
L+3	0.62	0	0	1	1	34	1	1	62
L+2	0.61	0	0	1	1	62	1	1	34
L+1	0.58	0	0	1	1	50	1	1	46
LUMO	0.56	0	0	1	1	46	1	1	50
HOMO	-6.72	4	4	17	18	11	17	18	11
H-1	-6.8	4	4	20	12	14	20	12	14
H-2	-7.16	3	3	10	34	5	9	31	5
H-3	-7.24	1	1	13	26	8	13	28	9
H-4	-7.27	3	4	9	27	9	10	29	9
H-5	-7.39	2	2	11	18	20	11	17	19
H-6	-7.55	1	0	0	4	50	1	4	41
H-7	-7.57	3	3	0	10	31	0	10	43
H-8	-7.61	2	2	6	11	31	7	10	31

Table S10. Selected vertical excitation energies computed by TD-DFT in CH₂Cl₂ with the orbitals involved for complexes **2** and **3**.

2			
	λ (nm)	f^a	Transition
S ₁	325	0.0835	HOMO->LUMO (32%), HOMO->L+2 (46%)
S ₂	323	0.034	HOMO->LUMO (45%), HOMO->L+2 (31%)
S ₃	318	0.113	H-1->L+1 (78%)
S ₄	314	0.0227	H-6->L+1 (10%), H-1->L+3 (75%)
S ₅	284	0.0843	H-4->L+3 (10%), H-3->L+1 (28%)
S ₆	283	0.1032	H-4->L+1 (46%), H-4->L+3 (14%)
S ₇	281	0.0654	H-2->L+2 (48%)
S ₈	279	0.0647	H-5->LUMO (18%), H-2->LUMO (21%), HOMO->L+4 (13%)
S ₉	278	0.0068	H-4->L+3 (34%), H-3->L+1 (19%)
S ₁₀	276	0.0221	H-3->L+3 (42%)
S ₁₁	274	0.0219	H-1->L+4 (30%)
S ₁₂	272	0.0257	HOMO->L+6 (25%)
S ₁₃	271	0.0159	H-9->L+2 (12%), H-5->L+2 (50%)
S ₁₄	270	0.2064	HOMO->L+6 (23%)
S ₁₅	270	0.2555	HOMO->L+5 (13%)
S ₁₆	269	0.1081	
S ₁₇	267	0.0741	HOMO->L+8 (12%)
S ₁₈	265	0.1929	H-9->L+2 (14%), H-7->L+2 (16%)
3			
	λ (nm)	f^a	Transition
S ₁	321	0.0748	H-1->LUMO (30%), HOMO->L+1 (27%)
S ₂	321	0.0424	H-1->L+1 (33%), HOMO->LUMO (26%)
S ₃	315	0.0417	H-1->L+2 (11%), H-1->L+3 (22%), HOMO->L+2 (24%)
S ₄	315	0.0384	H-1->L+2 (21%), H-1->L+3 (11%), HOMO->L+3 (26%)
S ₅	305	0.0179	HOMO->L+4 (47%), HOMO->L+12 (14%)
S ₆	296	0.0104	H-1->L+4 (51%), H-1->L+12 (10%)
S ₇	291	0.0901	H-3->L+4 (15%), H-2->L+4 (12%)
S ₈	281	0.4061	H-1->L+5 (22%), HOMO->L+7 (21%)
S ₉	280	0.0348	H-5->L+3 (10%)
S ₁₀	280	0.2523	H-1->L+7 (14%), HOMO->L+5 (18%)
S ₁₁	279	0.0856	H-4->L+2 (13%), H-2->L+3 (14%)
S ₁₂	278	0.0345	H-4->L+1 (16%), H-2->LUMO (11%), H-2->L+2 (10%)
S ₁₃	277	0.2094	H-4->LUMO (10%), H-2->L+1 (11%)
S ₁₄	274	0.0328	H-8->LUMO (11%)
S ₁₅	273	0.0791	H-8->L+3 (12%), H-3->L+3 (12%)
S ₁₆	271	0.018	H-5->LUMO (10%), HOMO->L+6 (21%)
S ₁₇	269	0.3241	H-7->LUMO (16%)
S ₁₈	269	0.0194	H-1->L+6 (21%), HOMO->L+8 (14%)

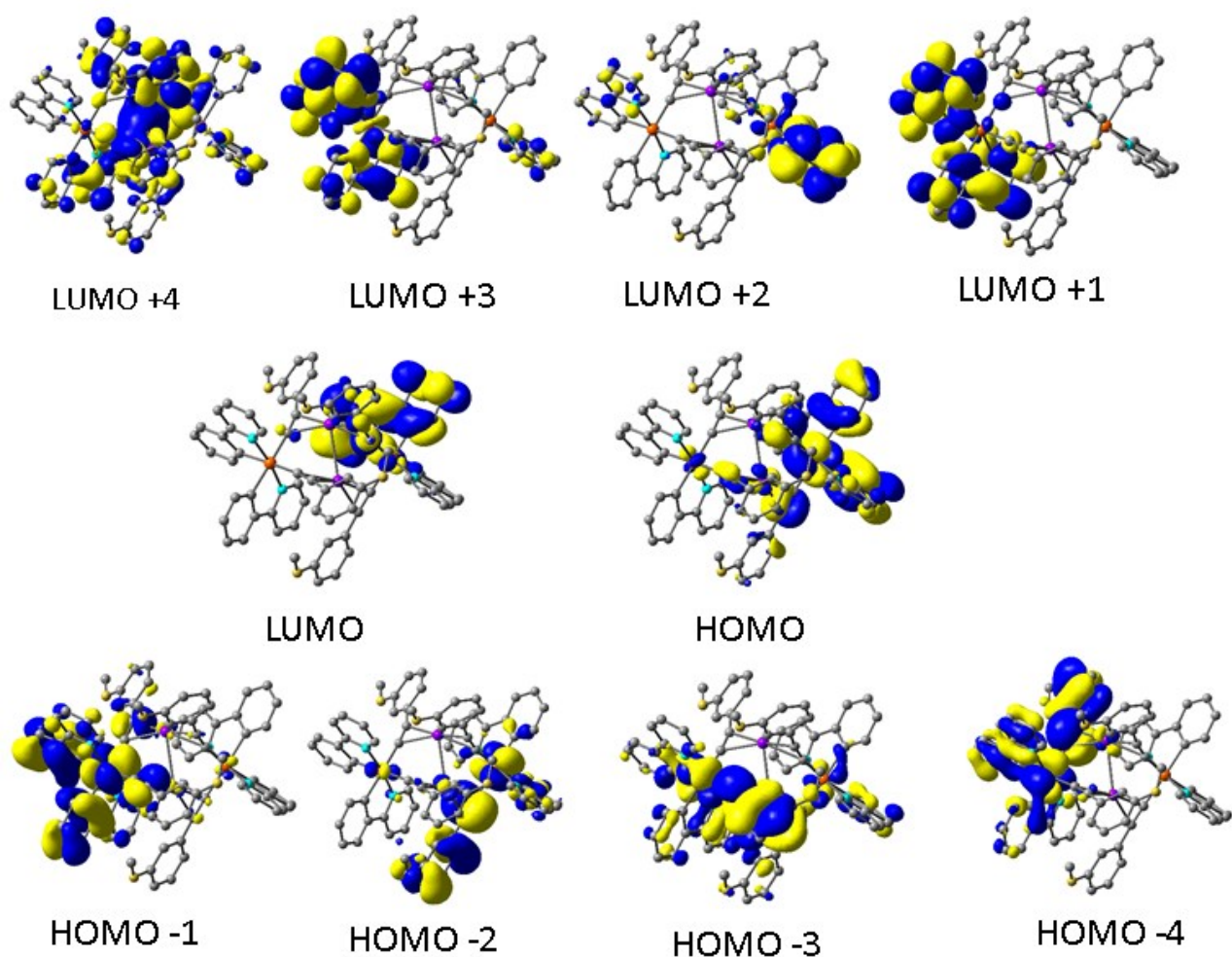


Fig. S28 Frontier MOs of **2** optimized in the ground state.

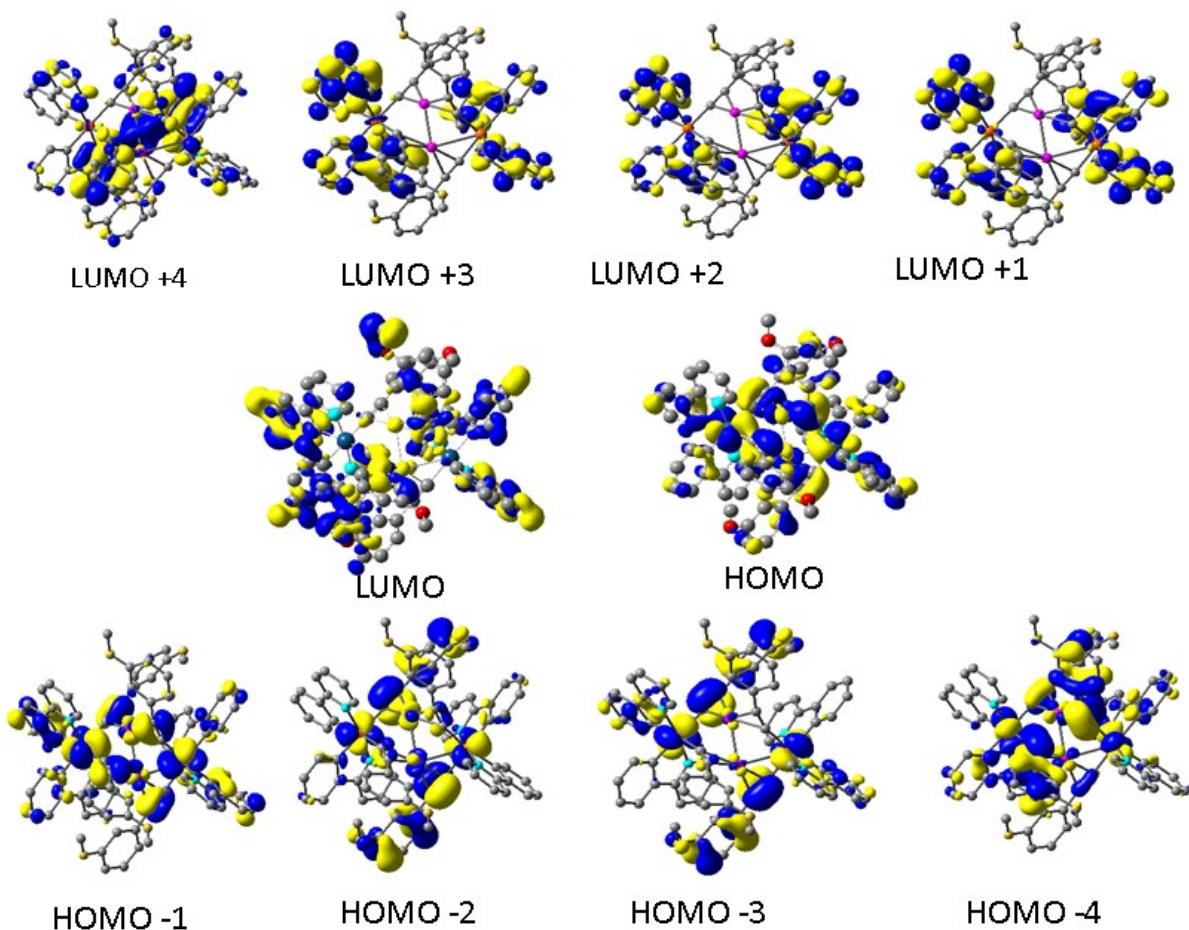


Fig. S29 Frontier MOs of **3** optimized in the ground state.

Table S11. Composition of Frontier Molecular Orbitals in the Triplet state for **2** and **3**

2	Ag(1)	Ag(2)	Ir(1)	C≡C(C ₆ H ₄ OMe-3) (Ir1)	ppy (Ir1)	Ir(2)	C≡C(C ₆ H ₄ OMe-3) (Ir2)	ppy (Ir2)
SOMO	0	0	3	1	95	0	1	0
SOMO-1	0	0	9	1	89	0	1	0
3	Cu(1)	Cu(2)	Ir(1)	C≡C(C ₆ H ₄ OMe-3) (Ir1)	ppy (Ir1)	Ir(2)	C≡C(C ₆ H ₄ OMe-3) (Ir2)	ppy (Ir2)
SOMO	7	6	0	3	1	4	73	6
SOMO-1	3	13	0	4	0	24	49	7

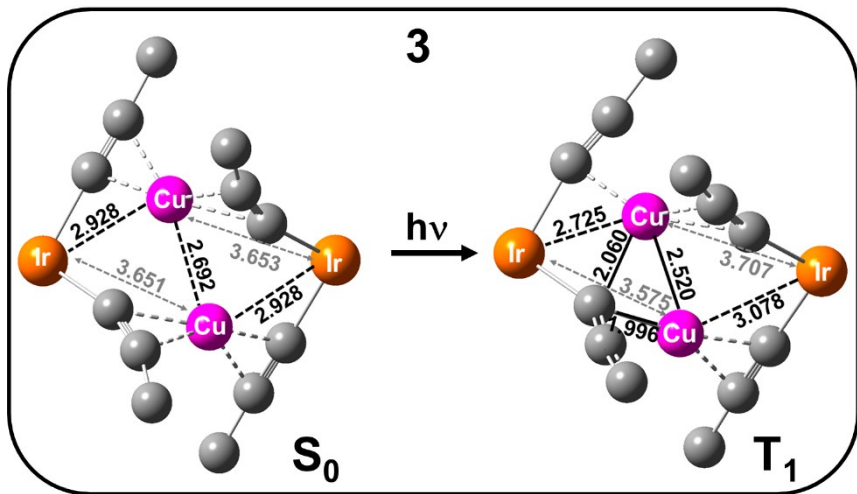


Fig. S30 Optimized structures (S_0 and T_1 state) in **3**. Distances are in Å